Author response to reviewer comments

Greg Tucker

May 2018

Note: in the following, each original reviewer comment is quoted in *italics*, and our response given in plain text.

Response to Reviewer 1 comments:

The main criticism on the paper relates to the model description. The authors present The Grain Hill model in Section 2 (?Model description?). This model builds on the previously introduced (slightly modified) CTS Lattice Grain model (Tucker et al., 2016) which is the main dynamical component of Grain Hill determining the movement of the grains on the hillslope. Although the authors have made some efforts to briefly describe this model component, I have found it insufficient. I am not claiming that the authors should provide all the details (again) of this model, since that description was the object of a previous publication, but given that the scope of the paper is introducing a new model for hillslope evolution (e.g. as indicated by the title), this paper should be sufficiently self-contained. What I mean is that the reader should have a good understanding of the functioning of the model (rules and dynamics) without the need of going back and forth between this manuscript and Tucker et al. (2016), which I have found myself doing quite often. Obviously, the technical implementation of the model rules (e.g., smart algorithms to rank times or how to take advantage of the Landlab?s grid architecture) can be omitted, since they are well described in the previous publication, and it is not detrimental to conveying the essence of the model.

This is a fair point, and we appreciate the value of having this paper be accessible on its own without forcing a reader to delve through the prior publication on CellLabCTS. In the revised manuscript, we have added text to the model description section that provides a more thorough explanation of the rules and how they function. Specific examples of changes made are given below in response to more detailed comments along these lines.

My understanding of the grain motion for the most basic grain dynamics of the model is as follows: (1) Disturbance is described as a Poisson process, assigning a state transition at a given time for every surface grain (random variable taken from an exponential distribution with parameter d), which forms a queue sorted by the transition times. (2) The ?soonest transition? (change in the state of the corresponding grain) in the queue is executed, which may trigger future state transitions of neighboring grains. (3) The gravity and inelastic

collision rules (Figure 4 and 5) would dictate the subsequent transitions and movements. I assume that the two latter processes (driven by gravity and collision) operate at smaller time scales. Is this so?

Yes, that is correct. We have added a new paragraph to section 2.1 to explain that each of the various transitions is represented as a Poisson process with a given rate constant. This paragraph briefly describes the "scheduling" process by which transitions are evaluated. We also added a short paragraph at the end of the section that notes the expectation of two distinct time scales.

What is the time scale of the gravitational transitions illustrated in figure 5? is that time scale dictated by an additional parameter/rate g (not listed in this manuscript)?

Yes, there is indeed an additional gravitational rate parameter. This parameter is the inverse of a gravitational settling time scale. Let's call this Tg. It represents the time it would take an initially stationary object to fall a distance of one cell (delta), assuming no fluid drag. Thus, g depends on the planet (we assume earth!) and on delta. To be exact, the time constant Tg = sqrt(2 delta/g). For most of the simulations shown in the paper, the cell size is assumed to be 0.1 m, and the corresponding Tg is 0.14 s, and the settling transition rate parameter is $\sim$7 s^{-1}. Because the time units in Grain Hill are taken to be years, the settling rate parameter is actually entered in units of inverse years: $1/Tg \sim 2.2 \times 10^{-7} y^{-1}$. The basis for the gravitational rate constant is now explained in section 2.1.

is g a constant rate, and therefore all the grains transition exactly at time 1/g after being updated to their current state? or is g the rate that characterizes an exponentially distributed random variable ?, and each grain transitions after a (different) lag ??

Excellent question. It is the second: gravitational settling is treated as a Poisson process, just like all other transitions in the model. This is now clarified in section 2.1. Admittedly, the stochastic treatment of grain settling raises the distinct possibility of having a grain hover in mid-air for a while before suddenly plunging downward (this is now acknowledged in the text). For our purposes, that's ok. What matters is that the grain-motion dynamics are fast relative to the "geomorphic" processes. This conclusion is backed up by informal sensitivity analysis, which shows that the choice of settling rate doesn't matter much as long as it is much shorter than the characteristic time scale for weathering, disturbance, and uplift relative to baselevel.

o What is the time scale at which the inelastic collisions and movements illustrated in figure 4 take place? Same than the previous time scale,1/g? constant lag or stochastic random variable?

Again, great question. Motion and collision transitions are both treated as stochastic. The model is built around the gravitational acceleration time scale. For the Grain Hill implementation, because collisions are assumed to be inelastic, the rate constant is the same as the gravitational rate constant. This is now explained in the revised version of the manuscript.

My understanding is that when a grain (or aggregate) moves to occupy an empty cell (fluid), it keeps the same state of movement (arrow direction). Is that correct?

Yes, that is correct. We have added a short paragraph explaining how motion works, including the fact that motion direction remains unchanged. As noted below, we also replaced one of the figures with a version that illustrates several different kinds of transition, including motion.

If yes, can this give rise to grains that temporally float in the fluid (grain surrounded by six fluid cells)? (I think it depends on the previous questions about the characteristic time scales of gravitational and movement/collision transitions).

Absolutely. This represents a grain in mid-trajectory. An example of this now appears in the new replacement figure.

How is the model initialized? For example, what is the geometry (flat?)? Do the lateral edges of the grid play a main role on the early evolution of the hillslope?

The model is initialized as mostly fluid, with regolith cells in the lowest two rows of the model domain (not including the left and right sides). The lower left and lower right cells are assigned to be rock, which represents the baselevel (and incidentally helps keep a consistent color scheme among different model configurations, because the rock state is always present). This is now explained in a the subsection "Initial and Boundary Conditions."

How does the grid type (squares vs. hexagons) affect the results? It is stated in page 7 (lines 12- 13) that the gravitational rule sets effectively the angle of repose to 30 degrees. Does the angle of repose strongly relate to the chosen hexagonal grid?

It is hard to answer this question definitively, because we have not tried running the model with a square lattice. Clearly, however, it is the combination of the hex grid and the down-and-to-the-side gravitational rule that imposes the 30 degree angle of repose. As the text notes, this restriction to 30 degrees is a limitation of the model. It could potentially be overcome by generalizing the transition rules to allow for a finite probability that a particular transition type will not take place at a particular location—and, in this particular example, that a spontaneous "sideways fall" will only occur with a probability P; otherwise, the material at that location is considered stable. One would then have two random variables associated with each transition type: one representing the probability that the transition will indeed occur at some future time, and (if that condition applies) the time in the future at which the transition will take place.

We should add that the hex geometry was chosen in part because it allows more axes of symmetry (3) than a square lattice (2). The alignment of the hex grid, with one axis vertical, was also deliberately chosen to allow for direct vertical fall of particles.

I would really appreciate as a reader to have access to some videos (as supplemental information) of the evolution of the model, including the evolution of the hillslope as it approaches its steady state.

Good idea. We have created five videos that will be added to the supplement.

Figure 3 is not very straightforward. Maybe it would be good to highlight the cell-pair affected by the transition/movement. With the current caption and text, it is confusing to see several arrows, but only one cell pair changing (this takes me back to my first questions about time scales). Also, I guess that this picture is not illustrative of the The Grain Hill model (otherwise some grains would be floating on the air/fluid). Maybe it would be more interesting to provide an example relevant to hillslopes.

We have replaced this with a figure that shows a sequence of transition events, and added explanatory text to the caption. This figure is now referred to in a couple of additional places in the text.

The authors illustrated in Figure 19 that the model is capable of reproducing realistic hillslope forms with parameters estimated from field data. However, it is not straightforward to evaluate the model performance in the absence of a direct comparison with the observations. I suggest that the authors can either (a) overlap Figure 19a,b with the profiles shown in Figure 2a,b to show that qualitatively the model is able to reproduce the form and height of those landforms, or (b) provide a quantification of the fit of the observed profile with the model results.

Good point. We have added the observed profiles to Figure 19.

Regarding the determination of the parameters, it may also be helpful if the authors can comment on their assumption of ?=1 m, as they suggested that the soil depths typically range between 0.2 and 1.2 m which is almost an order of magnitude difference for the variation. Are the results sensitive to this parameter?

We added a short paragraph summarizing the result of a sensitivity test on the Yucaipa example, which shows the one obtains the same shape and relief when delta is changed and the other parameters rescaled accordingly.

Figure 7 looks disproportionally big in comparison with other figures (e.g. Figure 4 or 5).

Figure 7 is meant to be a smaller, single-column figure. It is now re-scaled in the PDF file.

Please label the different panels of Figure 8 (e.g. a,b,...) to make easier their reference in the text.

We actually prefer not to do this, because the key text references to parts of this figure refer deliberately to geometric groupings: upper left, middle diagonal, lower right. If we labeled them with letters, readers would have to take time to work out which ones are a,b,d or f,h,i. The geometric references shouldn't be any more complicated (in fact, probably more intuitive), and it avoids cluttering the figure.

The authors state that Figure 9 shows the results of 125 model runs. It is not clear what those different runs are. From the figure, I can see 5x9 different combinations of ? and d so, do you run some cases twice and some case three times?

Added text here to explain that the 125 runs represent a 5x5x5 experimental grid, in which each grid point represents a particular combination of the three parameters d, τ, and λ.

Figure 19 caption: ?State state models? –¿ ?Steady state models?.
Fixed, thanks

Given the scope of the paper and the number of figures, I am not sure if Figure 6 adds much to the explanation of the model.

We think it is important to establish that the Lattice Grain model captures the essence of loose granular materials under gravity. We could simply refer to the original paper, but the reviewer noted above that it is easier if this piece can stand alone without the need to refer back to Tucker et al. (2016), so we prefer to keep this figure.

Please be consistent in terminology (e.g. mean gradient vs. slope gradient)

Thanks, fixed a few of these. However, there are places where the distinction between (local) slope gradient and mean slope gradient is important, so we've kept those as is.

The authors emphasize the simplicity of the model by pointing out the reduced number of parameters (3 in its simplest version). However, this kind of assessment is a little tricky when we refer to CA models, where the type and number of rules play a significant role in evaluating the simplicity of the model.

This is a fair point. The motion/gravitation rate can be thought of as a parameter, though as noted above, we think the model is insensitive to its value provided there is a clear gap between the "fast" and "slow" processes. Regarding the rules themselves, we regard these as being equivalent to terms in a traditional differential-equation model: they describe the physics rather than the rates (or length scales, etc.).

For me it is a little contradictory using ?continuous-time? and ?Cellular Automaton? as descriptors of a model. Cellular automata were originally defined as discrete models both in time and space, as well as the state variable of each grid cell. Models with discrete space and state variables, but continuous time, sometimes are called Boolean Delay Equations (Figure 2 in Zaliapin et al. 2003).

We appreciate hearing about this classification scheme. It seems, however, that there is not a consistent nomenclature. For example, Narteau and colleagues refer to their stochastic-in-time approach as a cellular automata, where Zaliapin would call it a Boolean Delay Equation. We can't be consistent with both at the same time, and in our earlier paper we called the approach a cellular automaton, so it seems best to stick with that terminology. However, we have added a nod to this with a sentence along the lines of: "A CTS model can be viewed as a type of Boolean Delay Equation (Ghil et al., 2008), though the number of possible states is not necessarily limited to just two."

Response to Reviewer 2 comments:

This manuscript describes a new method to simulate hillslopes based on a lattice- based cellular automaton framework. This work is highly innovative, clever, and won- derfully presented and I recommend publication given some minor considerations and clarifications that I?ll detail below.

First, though, I?ll note that this manuscript is situated on the cusp of invigorated efforts to revisit how our community does the accounting of mass on hillslopes. The continuum perspective that pervades so much of geophysical theory and simulation is being revisited to account for stochastic, nonlocal, and other effects and the approach adopted here complements forward-looking work by Furbish, Ganti, and others. While cellular automaton schemes have been around for some time, I am not aware of stud- ies that are so carefully crafted as this one as to allow for comparison and calibration with commonly used continuum parameters. This manuscript offers a clear roadmap for applying CA schemes to well-trod field sites and characteristic landforms.

Second, this manuscript is innovative not only for the algorithmic advances but the interpretations that emerge are also highly compelling. In particular, the ability of the model to account for disturbance processes as the source of both soil transport and production is conceptually appealing and a long-overdue advance. The continuum requirement of breaking up these processes has always been unsatisfying and this effort is to my knowledge the first to provide a unifying treatment. Also, the model?s ability to account for retreating cliff-rampart and rocky landforms is highly compelling. The authors neatly applied their toolkit to two field sites as a means to independently confirm their scaling arguments for the model parameters.

Third, (I?m still in gushing mode), I?ll note that the lattice grain model presented here is built on parsimony from the parameterization standpoint, which enables the authors to efficiently study a wide range of model outcomes.

Thanks for these comments! Indeed the approach has been inspired by advances in several directions, including recent efforts to understand what is sometimes called "stochastic transport" (as explored by the authors listed above, among others), as well as by our own frustrating experiences in trying to apply continuum theory to systems with complicated geometries and boundary conditions.

Below, I detail several comments for the authors to consider.

1) While the authors claim to invoke minimal parameters in defining their simulations, it seems that the choice of hexagon elements (which conveniently pack purely) as well as the myriad rules for different geometries constitute choices that impact the model outputs. For example, the hexagon packing results in a 30 degree angle of repose slope due to the geometry of the hexagon contacts as well as the gravity rules. This is an arbitrary choice that?s convenient for geometry and computational purposes. It turns out that 30 degrees is a fairly common friction angle for smooth cohesion grain piles, so this is appealing. That said, what prevents the model from being performed with octagons? In that case, the

packing isn?t as efficient and voids are required but it seems defensible nonetheless. Such a geometry would result in a 45 deg friction angle if the same rules were applied. Other element shapes and packing schemes are possible, in fact, a mind-boggling array could be tested. How does the choice of hexagons affect the results? Beyond setting the angle of repose, how do different packing schemes affect the rules for state changes (see below)?

It's a great question, and one that we have addressed to some extent above, in response to a similar comment from Reviewer 1. Simply put, we haven't studied other configurations. The most practical choices are squares or hexagons, and we picked hexagons because they offer an extra degree of geometric freedom. But it would be useful if there were a means to allow angle-of-repose behavior to reflect something other than grid geometry. To address this issue, the Discussion section notes the possibility of relaxing the 30 degree constraint with a "sticking rule". We added a comment along the lines of: "Such an enhancement might also make it possible for models with alternative lattice geometries to manifest the same dynamics, thereby de-coupling the basic model framework from the geometry of the lattice on which it is implemented." We hope this captures the spirit of the reviewer's point that the lattice is in a sense part of the model.

2) The rules of state changes are nicely laid out with an example orientation in figure 4, although it seems that some possible states are not represented and it would be nice if the figure was comprehensive given that no standards are offered as to why certain motion orientations result in motion and others do not. Can the authors write criteria for the outcomes of the inelastic collisions shown in Figure 4? In particular, the two particles that come together (far right) generate split 50/50 outcomes, why doesn?t the same type of outcome emerge with the far left shear-like interaction? I suspect that some of these details don?t matter terribly much but it?d be interesting to better understand which do matter and thus account for the behavior observed in the simulations. Is it possible to do an accounting of the state transformations and where they occur in order to determine which interactions dominate in the physical space of the model? Such an exercise is probably beyond the scope of this paper but it?d be very interesting to better understand the impact of the interaction choices listed here.

Indeed, the collision rules are somewhat arbitrary, and one could reasonably justify different rules from the ones illustrated here. For example, more of the collisions could lead both particles to halt (instead of just one), or conversely. We have not done comprehensive testing of these rules (other than to demonstrate that they lead to qualitative behavior that seems to mimic real sandpiles). There is certainly scope for a comprehensive sensitivity analysis of the collision rules, though not in this particular paper. We have added text in the model description section to the effect that: "The particular choices for frictional interaction are motivated simply by the geometry of the problem. They are non-unique in the sense that one could imagine reasonable alternatives to the rules illustrated in Figure **??**; however, the details of frictional interactions have little influence on the outcomes of the Grain Hill model."

3) I?m unclear on how the state transition occurs during a given time step. Given that state rules are only defined pair-wise, how are the transitions generated given that each element has 6 neighbors? How is precedence or primacy established? I?m certainly missing some aspect of how these calculations are performed, so perhaps a bit more explanation on this point is possible? Do the pair-state calculations actually occur in sequence? Or does the state transition happen simultaneously? If so, how are the particular pairs chosen? Or is every combination assessed?

As noted above in response to a comment by Reviewer 1, the model does not use time steps, but rather iterates through a series of asynchronous transition events. Text has now been added to the manuscript to explain this more clearly.

4) While the text addresses previous some work on soil-mantled slopes and transport models, the description of rocky slopes and cliff-rampart settings is lacking in scholar- ship and context. There?s a rich literature about cliff retreat in which conceptual models posed are likely consistent with the results generated here. Many workers, including Davis, King, Oberlander, Twidale, Ollier, and others have contemplated these land- forms with varying process models in mind, including and notably overland flow. Onlya very recent paper is cited here. The fact that the lattice grain model can generate iconic landforms without directly invoking overland flow is compelling and worth men- tion and/or context.

It's absolutely true that a lot has been written about rocky slopes in the "classic" literature. The problem is that there's so much that it would be impossible to summarize without detracting from the flow of the paper. To some extent, that literature is encapsulated in textbooks, but it doesn't feel right to quote a text. We chose the Howard and Selby paper is a fairly comprehensive review. In order to indicate that this is but one of many, we have now decorated that reference with "and references therein." We realize that this is not an ideal solution, but given that the main aim of this paper is to introduce the Grain Hill model as a concept, it seems like a reasonable shortcut. We envision a future paper that focuses less on the technique and more on the implications for rock slopes, where it would be appropriate to delve more deeply into the classic literature on such slopes.

5) The emergence of steady state rocky landforms for baselevel lowering rates that exceed the maximum soil production rate is perhaps the most attention-grabbing result of this model. The authors nicely describe how this results from slope and roughness, which is intuitive upon reflection. Given the importance of surface area for the total weathering flux, do any characteristic wavelengths emerge along the interface? is the roughness isolated to the element-scale or is it superimposed on broader wavelength fluctuations? It would be interesting to see if complexity (1/f noise or otherwise) of the surface emerges due to the need for weathering rates to keep pace. The possibility for feedbacks seems like fertile territory.

Great question. We haven't noticed emergence of characteristic wavelengths above the cell scale, but agree that this is fertile territory for future study.

6) The connection between disturbance and weathering through exposure is very ap-

pealing and nicely stated. In this sense, the creation of porosity and the evolution of that porosity in the regolith is a major conceptual advance. That said, it isn?t not clear to me in the text that porosity can be essentially advected to depth given a particular sequence of phase state changes. Is that the case? I?m not sure how else porosity goes downward, but however it does, it?s worth clarification b/c this sets the weather- ing rate along the bedrock interface. This goes back to the choices about pair-wise interactions. Would other choices for the interaction rules result in more/less porosity advection?

What a neat idea! It's a limitation of the model in its present form that there is no "explicit" porosity. Under the current rules, if a "pore cell" were to appear, it would rapidly be closed by collapse of the overlying particle. However, if one enhanced the rules with a "sticking probability", then conceivably one could have perfectly stable pores. Then one could actually begin to explore porosity advection. There might also need to be other, deeper changes, such as the use of larger cell neighborhoods (e.g., 6 cells instead of 2) in order to express cohesive bonding. We haven't tried to address this in the revised text, but would be eager to discuss these ideas further with the reviewer.

minor comments:

1) abstract: line 6: the concept of disturbances is part/parcel of this contribution and may merit mention in the abstract. Otherwise, the large block comment is unclear and is probably secondary in importance.

Good point – added text along the lines of: "Cells representing near-surface soil material undergo stochastic disturbance events, in which initially stationary material is put into motion and is statistically more likely to move downhill than uphill before coming to rest again. Net downslope transport emerges from the greater likelihood for disturbed material to move downhill than to move uphill. Cells representing rock undergo stochastic weathering events in which the rock is converted into regolith. "

2) pg 2, line 38ish: is it worth mentioning that the lattices don?t actually move but rather than the state evolves? it took me awhile to come around to this realization and it could be stated earlier in my opinion.

Great suggestion; now added a sentence to note this fact.

3) pg 4, line 20-25: the concept of state is employed here before it?s explained, I recommend moving some of the text from below (30-33 or so) upwards to clarify.

Added a bit of text here to indicate that a state is represented by an integer value at each cell.

4) pg 7, line 22: given the porosity, would it be possible to include water and a weathering function in the future?

That would probably require an additional set of rules. For example, it would probably be necessary to add a particle state that represents pore water or saturated soil. But in principle the framework could accommodate this sort of thing.

5) pg 10, line 16: given comments above about hexagon and friction angle, isn?t there really more than four parameters? I?m not sure how the counting works, but my sense is that the hillslope relief should depend on the angle of repose which results from hexagon worldview.

Fair enough, though we actually view the hex geometry as part of the "governing equation" rather than a parameter. Nonetheless, we nod to this issue in the Discussion section in a new sentence noting the desirability of de-coupling the model from the lattice geometry.

6) pg 13, figure 8: would it be possible to fit the standard paraboblic (and or nonlinear) analytical curves to these experimental profiles? that would be another way to determine the parameter scaling.

Actually, that's almost what we've done: we're fitting the average height of the standard parabolic curve to the average height in the experimental profiles. Text has now been added to point this out.

7) pg 14, eqn 13: I?m dim, but why is 3 on the denominator rather than 2? My apologies but whenever I?ve done this integration I end up with 2 on the bottom...please help.

It basically comes from integrating twice (once to go from slope to elevation profile, and a second time to get the average elevation). The derivation is:

$$\int_0^{\eta} = -(E/D_e) \int_{L_h}^{x} x dx \rightarrow \tag{1}$$

$$\eta - 0 = -(E/D_e)(x^2/2 - L_h^2/2) \rightarrow \tag{2}$$

$$\eta = (E/2D_e)(L_h^2 - x^2) \tag{3}$$

That's the parabolic profile. Then integrate to get the average height:

$$\bar{\eta} = (1/L_h)(E/2D_e)[\int_0^{L_h} L_h^2 dx - int_0^{L_h} x^2 dx] \rightarrow \tag{4}$$

$$\bar{\eta} = (1/L_h)(E/2D_e)[L_h^3 - L_h^3/3] \rightarrow \tag{5}$$

$$\bar{\eta} = (1/L_h)(E/2D_e)(2/3)L_h^3 \rightarrow \tag{6}$$

$$\bar{\eta} = (E/3D_e)L_h^2 \tag{7}$$

8) pg 19, figure 13: it?s difficult to see the various symbols here.

Yes, that's true—many are over-printed because they fall right on the 1:1 line. Because there's no obvious way to correct this on the plot itself, we have added a line of text pointing out to the reader that some of the lower-quintile points are obscured by being over-plotted right on the 1:1 line.

9) pg 20, line 4: isn?t the creation of porosity and it?s downward advection akin to a depth-dependent process? the text here seems restrictive.

Porosity is only being created indirectly, through the process of rock-to-regolith conversion (as opposed to being explicitly represented by fluid cells in the subsurface). Under the rules presented here, rock-to-regolith conversion only happens where a rock cell meets a fluid cell, which is why we say here that the model doesn't capture weathering processes that extend deeper than one cell at any given moment. However, the caveat "present configuration" is meant to signal that one COULD develop more sophisticated rules that would relax this limitation. For example, you might introduce a "saturated regolith" condition that could move downward (representing infiltration) or perhaps upward (representing capillary suction). One could then introduce a transition wherein the pairing of rock with saturated regolith transitions to two regolith (wet or dry) cells, representing subsurface chemical weathering.

10) 7) The diffusivity values for Gabilan Mesa seem quite high and I wonder if this results from K calibration using low-curvature hilltops that are not reflective of integrated erosion in that site.

The value is indeed on the high end, though not off the charts (McKean et al.'s estimate from the Black Diamond Reserve in CA was 0.036 m2/yr). We estimated a profile-averaged effective transport coefficient. The Gabilan profiles are not perfectly parabolic and would be best fit by a slightly nonlinear transport rule. The slightly high D reflects this. A transport coefficient obtained by only fitting the constant curvature hilltops is indeed lower than what we report for the profile-averaged value.

A lattice grain model of hillslope evolution

Gregory E. Tucker[1], Scott W. McCoy[2], and Daniel E.J. Hobley[3]

[1]Cooperative Institute for Research in Environmental Science (CIRES) and Department of Geological Sciences, University of Colorado, Boulder, CO 80305 USA
[2]Department of Geological Sciences and Engineering, University of Nevada, Reno, NV, 89557 USA
[3]School of Earth and Ocean Sciences, Cardiff University, Cardiff CF10 3AT Wales

Correspondence to: Greg Tucker (gtucker@colorado.edu)

Abstract. This paper describes and explores a new continuous-time stochastic cellular automaton model of hillslope evolution. The Grain Hill model provides a computational framework with which to study slope forms that arise from stochastic disturbance and rock weathering events. The model operates on a hexagonal lattice, with cell states representing fluid, rock, and grain aggregates that are either stationary or in a state of motion in one of the six cardinal lattice directions. Cells representing near-surface soil material undergo stochastic disturbance events, in which initially stationary material is put into motion. Net downslope transport emerges from the greater likelihood for disturbed material to move downhill than to move uphill. Cells representing rock undergo stochastic weathering events in which the rock is converted into regolith. The model can reproduce a range of common slope forms, from fully soil mantled to rocky or partially mantled, and from convex-upward to planar shapes. An optional additional state represents large blocks that cannot be displaced upward by disturbance events. With the addition of this state, the model captures the morphology of hogbacks, scarps, and similar features. In its simplest form, the model has only three process parameters, which represent disturbance frequency, characteristic disturbance depth, and baselevel lowering rate, respectively. Incorporating physical weathering of rock adds one additional parameter, representing the characteristic rock weathering rate. These parameters are not arbitrary but rather have a direct link with corresponding parameters in continuum theory. Comparison between observed and modeled slope forms demonstrates that the model can reproduce both the shape and scale of real hillslope profiles. Model experiments highlight the importance of regolith cover fraction in governing both the downslope mass transport rate and the rate of physical weathering. Equilibrium rocky hillslope profiles are possible even when the rate of baselevel lowering exceeds the nominal bare-rock weathering rate, because increases in both slope gradient and roughness can allow for rock weathering rates that are greater than the flat-surface maximum. Examples of transient relaxation of steep, rocky slopes predict the formation of a regolith-mantled pediment that migrates headward through time while maintaining a sharp slope break.

1 Introduction

Hillslopes take on a rich variety of forms. Their profile shapes may be convex-upward, concave-upward, planar, or some combination of these. Some slopes are completely mantled with soil, whereas others are bare rock, and still others draped

in a discontinuous layer of mobile regolith. The processes understood to be responsible for shaping them are equally varied, ranging from disturbance-driven creep to dissolution to large-scale mass movement events.

Considerable research has been devoted to understanding the evolution of soil-mantled slopes that are primarily governed by disturbance-driven creep, such as down-slope soil transport by biotic and abiotic soil-mixing processes. As a result, the geomorphology community has mathematical models that account well for observed slope forms and patterns of regolith thickness (e.g., Roering, 2008). Furthermore, stochastic-transport theory provides a mechanistic link between the statistics of particle motion, the resultant average rates of downslope transport, and the emergence of convex-upward, soil-mantled slope forms (Culling, 1963; Roering, 2004; Foufoula-Georgiou et al., 2010; Furbish et al., 2009; Furbish and Haff, 2010; Tucker and Bradley, 2010).

One gap that remains, however, lies in understanding steep, rocky slopes (Figure 1). "Rocky" implies slopes that lack a continuous soil cover ~~(Howard and Selby, 1994)~~(e.g., Howard and Selby, 1994, and references therein); here, transport laws that assume the existence of such a cover no longer apply. "Steep" implies angles approaching or exceeding the effective angle of repose for loose, granular material, so that ravel may be an important transport mode (e.g., Gabet, 2003; Roering and Gerber, 2005; Lamb et al., 2011; Gabet and Mendoza, 2012) and particles have the potential to fall as soon as they are released from bedrock. This type of relatively fast, long-distance transport does not fit comfortably in the framework of standard diffusion-based models of hillslope soil transport, which derive from an underlying assumption that the characteristic length scale of motion is short relative to the length of the slope.

Rocky slopes are rarely completely barren. More commonly, they have a patchy cover of loose material, which may either retard rock weathering by shielding the rock surface from moisture or temperature fluctuations, or enhance it by trapping water and allowing limited plant growth. A discontinuous cover does not fit easily within the popular exponential-decay regolith-production models (e.g., Heimsath et al., 2012; Lamb et al., 2013), which assume an essentially continuous soil mantle.

An additional issue, which pertains to both rocky and soil-mantled slopes, is the connection between sediment movement at the scale of individual "motion events," and the resulting longer-term average sediment flux, which forms the basis for continuum models of hillslope evolution. Recent theoretical and experiment work has begun to forge a mechanistic connection between these scales (Culling, 1963, 1965; Furbish et al., 2009; Furbish and Haff, 2010; Tucker and Bradley, 2010; Gabet and Mendoza, 2012; Lamb et al., 2013). However, the community's resources for computational analysis of particle-level dynamics remain limited, lagging behind developments in understanding sediment transport in coastal environments (Drake and Calantoni, 2001) and rivers (McEwan and Heald, 2001; MacVicar et al., 2006; Furbish and Schmeeckle, 2013; Schmeeckle, 2014).

To further our understanding of how grain-level weathering and transport processes translate into hillslope evolution, both for hillslopes in general and rocky slopes in particular, it would be useful to have a computational framework with which to conduct experiments. Ideally, such a framework should be sophisticated enough to capture the essence of weathering and granular mechanics, while remaining simple enough to involve only a small number of parameters and provide reasonable computational efficiency.

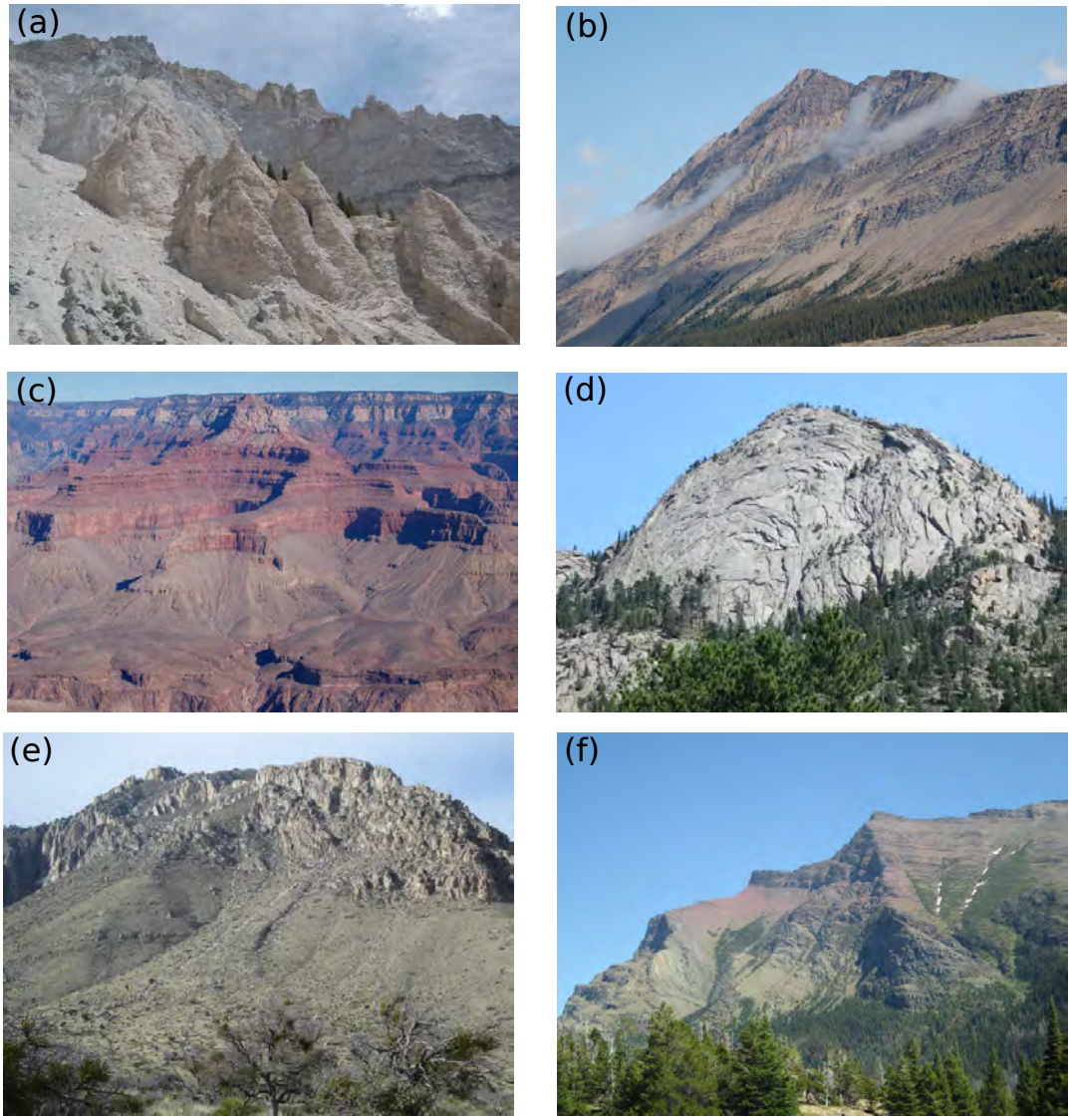

Figure 1. Examples of rocky hillslopes, sometimes referred to as Richter slopes. (a) Chalk Cliffs, Colorado, USA. (b) Canadian Rockies. (c) Grand Canyon, Arizona, USA. (d) Rocky Mountain National Park, Colorado, USA. (e) Guadeloupe Mountains, Texas, USA. (f) Waterton Lakes National Park, Canada (photos by G.E. Tucker).

Our aim in this paper is to describe one such computational framework, test whether it is capable of reproducing commonly observed hillslope-profile forms, and examine how its parameters relate to the bulk-behavior parameters used in conventional continuum models of soil creep and regolith production. The model uses a pairwise, continuous-time stochastic (CTS) approach to combine a Lattice Grain model with rules for stochastic bedrock-to-regolith conversion ("weathering") and disturbance of

surface regolith particles. One goal of this event-based approach is to study how bulk behavior, such as the diffusion-like net downslope transport of soil, can emerge from a large ensemble of stochastic events. In this paper, we present the "Grain Hill" model, and examine its ability to reproduce three common types of slope profile: (1) convex-upward, soil-mantled slopes (Figure 2a,b), (2) quasi-planar rocky slopes (Figure 2c,d), and (3) cliff-rampart morphology in layered strata (Figure 2e,f).

We begin with a description of the modeling technique. We then present results that illustrate the macroscopic behavior of the model under a variety of boundary conditions, and define the relationship between the cellular model's parameters and the parameters of conventional continuum mechanics models for hillslope evolution.

2 Model Description

The model combines a cellular automaton representation of granular mechanics with rules for weathering of rock to regolith and for episodic disturbance of regolith. Cellular automata are widely used in the granular mechanics community, because they can represent the essential physics of granular materials at a reasonably low computational cost. Because the principles are often similar to those of lattice-gas automata in fluid dynamics (e.g., Chen and Doolen, 1998), cellular automata for granular mechanics are sometimes referred to as Lattice Grain models (LGrMs) (Gutt and Haff, 1990; Peng and Herrmann, 1994; Alonso and Herrmann, 1996; Károlyi et al., 1998; Károlyi and Kertész, 1999, 1998; Martinez and Masson, 1998; Désérable, 2002; Cottenceau and Désérable, 2010; Désérable et al., 2011).

2.1 CTS Lattice Grain Model

Our approach starts with a two-dimensional (2D) continuous-time stochastic ("CTS") Lattice Grain cellular automaton. A cellular automaton can be broadly defined as a computational model that consists of a lattice of cells, with each cell taking on one of N discrete states (represented by an integer value). These states evolve over time according to a set of rules that describe transitions from one state to another as a function of a particular cell's immediate neighborhood. A continuous-time stochastic model is one in which the timing of transitions is probabilistic rather than deterministic. Whereas transitions in traditional cellular automata occur in discrete time steps, in a CTS model they are both stochastic and asynchronous. A CTS model can be viewed as a type of Boolean Delay Equation (Ghil et al., 2008), though the number of possible states is not necessarily limited to just two.

The method we present here, which we will refer to as the Grain Hill model, is implemented in the Landlab modeling framework (Hobley et al., 2017). The Lattice Grain component, on which Grain Hill builds, is described in detail by Tucker et al. (2016). Here we present only a brief overview of the Lattice Grain model's rules and behavior. The framework is based on the pairwise ("doublet") method developed by Narteau and colleagues (Rozier and Narteau, 2014), which has been applied to problems as diverse as eolian dune dynamics (Narteau et al., 2009; Zhang et al., 2010, 2012) and the core-mantle interface (Narteau et al., 2001).

In the basic CTS Lattice Grain model, the domain consists of a lattice of hexagonal cells. Each cell is assigned one of eight states (Table 1, states 0–7). These states represents the nature and motion status of the material: state 0 represents fluid (an

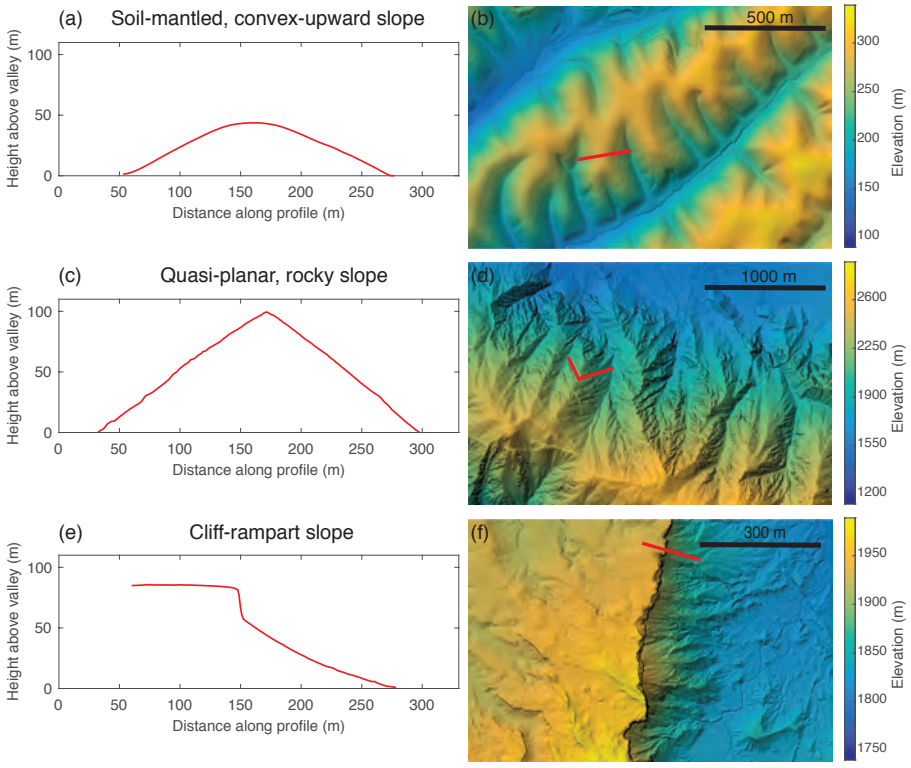

Figure 2. Examples of three characteristic types of hillslope profile. Red line in mapview depicts hillslope profile location. (a, b) Soil-mantled, convex-upward slope (Gabilan Mesa, California, USA). (c, d) Quasi-planar, thinly mantled slope (Yucaipa Ridge, California, USA). (e, f) Cliff formed in resistant Tertiary laccolithic intrusive rocks overlying Jurassic sedimentary rocks (Cedar Mountain, Utah, USA).

Table 1. States in the Grain Hill model.

State	Description
0	Fluid
1	Grain moving upward
2	Grain moving up and right
3	Grain moving down and right
4	Grain moving down
5	Grain moving down and left
6	Grain moving up and left
7	Resting grain
8	Rock
(9)	Block (optional)

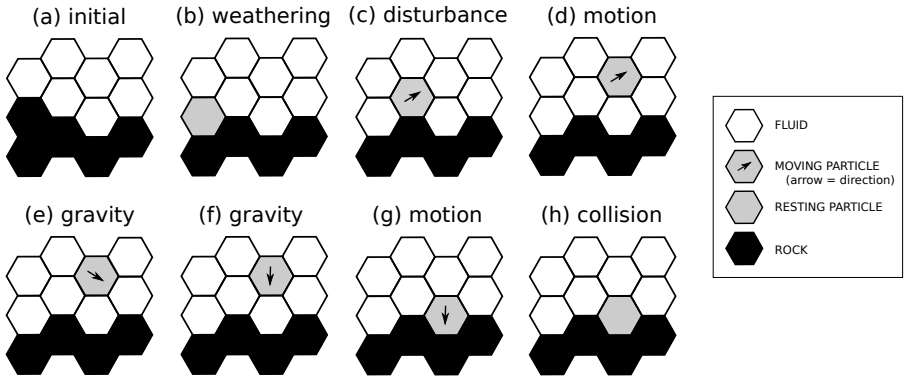

Figure 3. ~~Example~~ Hypothetical time sequence of ~~a four-by-four lattice~~transition events, from upper left to lower right, illustrating several of the ~~first nine~~ states and transitions in the Grain Hill model~~and including an~~ . Note that although this example ~~transition in which~~ shows a ~~falling grain trades places with the fluid cell below~~ single particle in motion, it is possible for multiple cells to exist in a state of motion at any given time.

"empty" cell into which a solid particle can move), states 1–6 represent a grain moving in one of the six lattice directions, and state 7 indicates a stationary grain (or aggregate of grains, as discussed below). For purposes of modeling hillslope evolution, we add an additional state (8) to represent rock, which is immobile until converted to granular material, representing regolith. An optional additional state (9) is used to model large blocks, as described below. Figure 3 ~~illustrates states 0–8, with an example of a single transition in which a falling grain switches places with the fluid cell below it~~shows several of these states in the form of a time sequence of transition events. Note that the timing of transition events is purely stochastic; there are no time steps in the usual sense.

Like other Lattice Grain models, the CTS Lattice Grain model is designed to represent, in a simple way, the motion and interaction of an ensemble of grains in a gravitational field. The physics of the material are represented by a set of transition rules, in which a given adjacent pair of states is assigned a certain probability per unit time of undergoing a transition to a different pair. For example, consider a vertically aligned pair of cells in which the top cell has state 4 (moving downward) and the bottom cell state 0 (empty/fluid) (Figure 3~~, leftf~~). Downward motion (falling) is represented by a transition in which the two states switch places (Figure 3~~, right).~~ g).

The stochastic pairwise transitions in the CTS Lattice Grain model are treated as Poisson processes. The probability density function for the waiting time, t, to the next transition event at a particular pair is given by an exponential function with a rate parameter r, which has dimensions of inverse time:

$$p(t) = re^{-rt}. \tag{1}$$

Each transition type is associated with a rate parameter that represents the speed of whichever process the transition is designed to represent. To implement these transitions, the CTS Lattice Grain model steps from one transition to the next, rather than iterating through time steps of fixed duration. Whenever the state of one or both cells in a particular pair changes, if the new pair is subject to a transition, the time at which the transition is scheduled to occur is added to a queue of pending events. The soonest among all pending events is chosen for processing, and the process repeats until either the desired run time has completed or there are no further events in the queue. Further details on the implementation and algorithms are provided in Tucker et al. (2016).

Grain motion through fluid is represented by a transition involving a moving grain and an adjacent fluid cell in the direction of the grain's motion: the two cells exchange states, representing the motion of the grain into the fluid-filled cell, and the replacement of the grain's former location with fluid (Figure 3, c-d and f-g). During this transition, the grain's motion direction remains unchanged (Figure 4, top left). Note that the lattice itself never moves; rather, material motion is represented simply by an exchange of grain and fluid states between an adjacent pair of cells.

Gravity is represented by transitions in which a rising grain decelerates to become stationary, a stationary grain accelerates downward to become a falling particle, and a grain moving upward at an angle accelerates downward to move downward at an angle (Figure 5). An additional rule allows for acceleration of a particle resting on a slope: a stationary particle adjacent to a fluid cell below it and to one side may transition to a moving particle (Figure 5, bottom row). Importantly for our purposes, this latter rule effectively imposes an angle of repose at 30°.

For gravitational transitions, the rate parameter, r_g, is determined by considering the time it would take for an initially stationary object to fall a distance of one cell width under gravitational acceleration without fluid drag. This works out to be

$$r_g = \sqrt{2\delta/g}, \tag{2}$$

where δ is cell width and g is gravitational acceleration. This rate parameter is used for all of the gravitational transitions illustrated in Figure 5.

Because of the stochastic treatment of all transitions—including gravitational ones—it is possible for grains in the model to hover in mid-air for a brief period of time before plunging downward (e.g., Coyote, 1949). For purposes of modeling hillslope

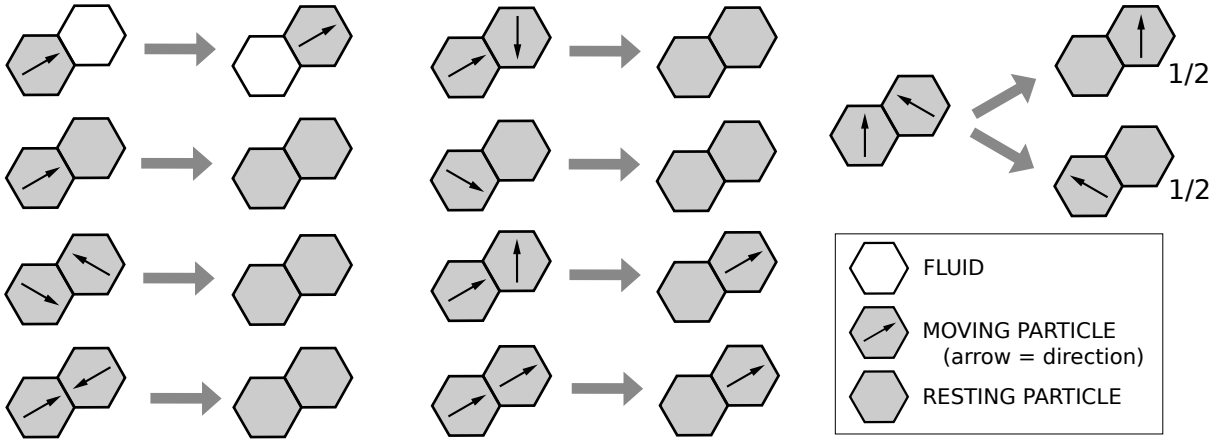

Figure 4. Rules for motion and frictional (inelastic) collisions, illustrated here for one of the six lattice directions.

evolution, this is fine; what matters most is that there is a distinct time-scale gap between "fast" (large rate constant) processes associated with grain motion, and "slow" (small rate constant) processes associated with weathering and disturbance, which are described below. First, however, we must consider frictional interactions among moving particles.

We assume that biophysical disturbance events such as the growth of roots and burrowing by animals, and the settling motions that follow, tend to impart low kinetic energy, with "low" defined as ballistic displacement lengths that are short relative to hillslope length and comparable to or less than the characteristic disturbance-zone thickness. We consider such motions to be dominated by frictional dissipation rather than by transfer of kinetic energy by elastic impacts. This view is similar to the reasoning of Furbish et al. (2009) that the mean-free-path of mobile grains will typically be short relative to hillslope length, scaling with the grain radius and particle concentration. For this reason, unlike the original Lattice Grain model of Tucker et al. (2016), ~~we consider here~~ the present formulation includes only inelastic collisions (Figure 4). These inelastic (frictional) collisions are represented by a set of rules in which one or both colliding particles become stationary, representing loss of momentum and kinetic energy as a result of the collision. ~~Gravity is represented by transitions in which a rising grain decelerates to become stationary, a stationary grain accelerates downward to become a falling particle, and a grain moving upward at an angle accelerates downward to move downward at an angle (Figure 5). An additional rule allows for acceleration of a particle resting on a slope: a stationary particle adjacent to a fluid cell below it and to one side may transition to a moving particle (Figure 5, bottom row). Importantly for our purposes, this latter rule effectively imposes an angle of repose at 30°~~The particular choices for frictional interaction are motivated simply by the geometry of the problem. They are non-unique in the sense that one could imagine reasonable alternatives to the rules illustrated in Figure 4; however, the details of frictional interactions have little influence on the outcomes of the Grain Hill model. In the general Lattice Grain CTS model, the rate parameter for frictional transitions is set equal to the product of the gravitational parameter and a dimensionless friction factor, $f \in [0,1]$ (there is also a corresponding elastic factor equal to $1 - f$). In the Grain Hill implementation explored in this paper, $f = 1$, such that particle collisions are purely frictional.

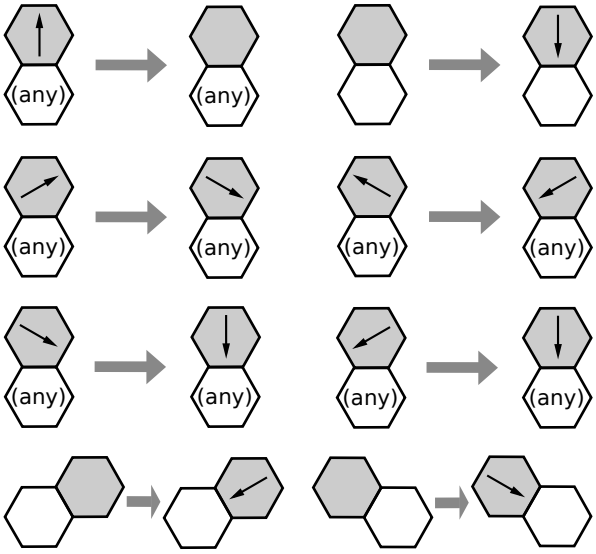

Figure 5. Illustration of gravitational rules. The bottom row shows the "falling on a slope" rule, which effectively imposes a 30° angle of repose. Modified from Tucker et al. (2016).

One limitation of the CTS Lattice Grain model is that falling grains do not accelerate through time; instead, they have a fixed transition probability that implies a statistically uniform downward fall velocity. This treatment is obviously unrealistic for particles falling in a vacuum, though it is consistent with a terminal settling velocity for grains immersed in fluid. Consistent with the above reasoning, the relatively short ballistic displacement lengths asserted for the modeled hillslopes also reduce the importance of this assumption, as a particle would typically have little time to accelerate before impacting another particle.

Tests of the CTS Lattice Grain model show that it reproduces several basic aspects of granular behavior (Tucker et al., 2016). For example, when gravity and friction are deactivated, the model conserves kinetic energy. When gravity and friction are active, the model reproduces some of the common behaviors observed with granular materials. For example, Figure 6 illustrates a simulation of the emptying of a silo to form an angle-of-repose grain pile. For our purposes, what matters most is simply that the model captures, in a reasonable way, the response of particles on a slope to episodic disturbance events.

2.2 Weathering and Soil Creep

Weathering of rock to form mobile regolith is modeled with a transition rule: when a rock cell lies adjacent to a fluid cell (which here is assumed to be air), there is a specified probability per unit time, w [1/T], of transition to a grain-air pair (Figure 3a-b, and Figure 7, top). In other words, w is the Poisson rate constant for the weathering transition process. This treatment means that the effective maximum expected weathering rate, in terms of the propagation of a weathering front, is cell diameter, δ, times w. An indirect consequence of this approach is that the weathering rate declines with increasing regolith thickness. As average regolith thickness increases, the fraction of the surface where rock is in contact with air diminishes, and consequently

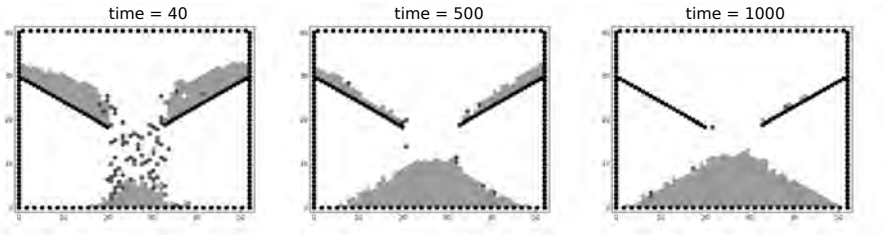

Figure 6. Lattice Grain simulation of emptying of a silo. Light-shaded grains are stationary; darker-shaded ones are in motion. Black cells are walls (rock). From Tucker et al. (2016).

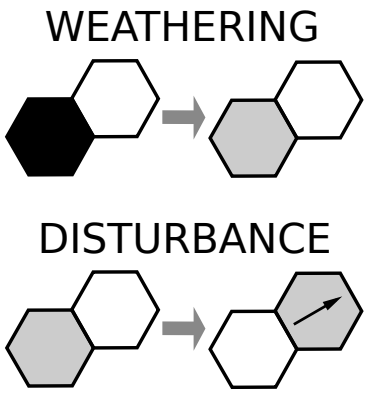

Figure 7. Transitions representing rock-to-regolith transformation by weathering (top), and regolith disturbance (bottom), in which a stationary particle becomes mobile and switches position with a air cell. Illustration represents one of the six possible orientations.

so too does the average transition rate. A limitation of the approach is that when the rock is completely mantled, no further weathering can take place. We explore the consequences of this rule below, and compare it with the behavior of continuum regolith-production models.

Soil creep is modeled by a transition rule that mimics the process of episodic disturbance of the mobile regolith (which we use here as a generic term that includes various forms of unconsolidated granular material, such as soil, colluvium, and scree). For each resting grain that is adjacent to an air cell, there is a specified probability per unit time, d [1/T], that the regolith and air will exchange places, representing movement (Figure 3b-c). The regolith cell is also converted from a stationary state to a state of motion (Figure 7, bottom). An advantage of this approach is that it mimics, in a general way, the effectively stochastic disturbance processes that are understood to drive soil creep.

Our definition of d is closely related to the activation rate, N_a, in the probabilistic theory for soil creep developed by Furbish et al. (2009). When combined with the Lattice Grain gravitational rules, the resulting cellular model captures both the scattering (disturbance) and settling (gravitational) behavior articulated by Furbish et al. (2009). In the Grain Hill cellular model, as in their theory, downslope regolith flux arises because, on average, scattering occurs normal to the local surface while setting

is vertical. The Grain Hill model includes an additional element not present in the Furbish et al. (2009) theory: an increase in (downward) scattering distance for particles on slopes steeper than 30°. This behavior, as illustrated below, promotes a nonlinear relationship between gradient and flux, and leads to the possibility of threshold slopes.

Note that the weathering and disturbance rate constants (w and d, respectively) are understood to be considerably smaller than the gravitational rate constant, r_g. As noted above, a key concept here is that there are two distinct time scales: a short time scale associated with grain motion, and a much longer scale associated with weathering and disturbance frequency.

2.3 Cells as Grain Aggregates

Natural regolith disturbance events usually impact many grains at once. Raindrop impacts on bare sediment typically dislodge several grains at once (Furbish et al., 2007). Excavation of an animal burrow disturbs a volume a grains equal to the volume of the burrow, and the fall of a tree mobilizes a volume of regolith similar to the volume of the tree's root mound. Observations of such processes suggest that there may be a characteristic volume of disturbance that in some cases may be much larger than the volume of a single grain. For this reason, we envision regolith cells as being grain aggregates, with a length scale (width of a cell) δ and a volume scale δ^3.

2.4 Initial and Boundary ~~conditions~~Conditions

The 2D model domain ~~consists of a~~ represents the cross-section of a hypothetical hillslope, on which particles move within the cross-sectional plane. Any regolith cells that reach the model's side or top boundaries disappear. This treatment is meant to represent the presence of a stream channel at the base of each side of the model hillslope; particles reaching these channels are assumed to be eroded. Progressive lowering of baselevel at the two model boundaries is treated by moving the interior cells upward away from the lower boundary, and adding a new row of rock or regolith cells along the bottom row. A new row of cells is added at time intervals of τ.

Cells around the lattice perimeter retain their initial states. If, for example, a transition occurs in which a grain "moves" into a fluid cell on the lattice perimeter, its former location will correctly transition to a fluid cell, but the perimeter cell itself will retain its status as a fluid cell. Effectively, this treatment means that grains or blocks reaching either of the two vertical boundaries are instantly eroded.

The initial condition for most runs presented here has the bottom two rows filled with regolith grains. The lower left and lower right cells are assigned to be rock, which represents the baselevel (and incidentally helps keep a consistent color scheme among different model configurations, because the rock state is always present). The rest of the domain is initialized as air cells.

2.5 Scaling and Nondimensionalization

The basic model has four parameters: the disturbance rate, d [cells/T], weathering rate, w [cells/T], baselevel lowering interval, τ [T], and width of domain, λ [cells]. The baselevel lowering timescale τ represents the time interval between episodes of

relative uplift in which the interior domain is lifted by one cell relative to its side boundaries. The domain width might properly be considered a boundary condition rather than a parameter, but we include it here with an eye toward examining how slope width impacts hillslope properties such as mean height. Once we define the width of a cell, δ [L], we can define versions of these four parameters that explicitly incorporate this length scale:

$$D = d\delta, \tag{3}$$

$$W = w\delta, \tag{4}$$

$$U = \delta/\tau, \tag{5}$$

$$L = \lambda\delta. \tag{6}$$

Consider the case of dynamic equilibrium, in which the rate of baselevel lowering is balanced by the hillslope's rate of erosion. The mean height of this steady state hillslope, H, is a function of the above four parameters plus the characteristic length scale δ, such that we end up with a total of six variables:

$$H = f(D, W, U, L, \delta). \tag{7}$$

Buckingham's Pi Theorem dictates that these six variables, which collectively include dimensions of length and time, may be grouped into four dimensionless quantities:

$$\frac{H}{\delta} = f\left(\frac{D}{U}, \frac{W}{U}, \frac{L}{\delta}\right) \tag{8}$$

The ratio $d' = d\tau = D/U$ is a dimensionless disturbance rate. Similarly, $w' = w\tau = W/U$ is a dimensionless weathering rate. Noting the definitions above, equation (8) is equivalent to

$$h = f\left(d', w', \lambda\right), \tag{9}$$

where $h = H/\delta$ is dimensionless hillslope height. Hence, we have a dimensionless property of the hillslope, h, that depends uniquely on three other non-dimensional variables, representing disturbance rate, weathering rate, and length.

One can similarly define a dimensionless regolith thickness, $r = R/\delta$, where R is the dimensional equivalent; it too should depend on the three dimensionless parameters that represent disturbance rate d', weathering rate, w', and hillslope length, λ, respectively. For a hillslope composed entirely of regolith, r and h depend solely on d' and λ. Finally, we define a fractional regolith cover F_r. In the Grain Hill model, F_r is calculated as the number of air-regolith cell pairs divided by the total number of cell pairs that juxtapose air with either regolith or rock.

2.6 Blocks

The foregoing model is designed to represent regolith as grain aggregates composed of gravel-sized and finer grains: material fine enough that it is susceptible to being moved by processes such as animal burrowing, frost heave, tree throw, and so on. Some hillslopes, however, are adorned with grains that are simply too large to be displaced significantly by such processes. For

example, Glade et al. (2017) presented a case study and model of slopes formed beneath a resistant rock unit that periodically sheds meter-scale or larger blocks. On at least some of these types of slope, the distance between surface blocks and their source unit is considerably greater than the distance that they could roll during an initial release event (Duszyński and Migoń, 2015). This observation implies that the blocks are transported down slope by a process of repeated undermining. Glade et al. (2017) hypothesized that erosion of soil beneath and immediately downhill can cause a block to topple, and hence move a distance comparable to its own diameter in each such event.

We wish to capture this form of "too big to disturb" behavior in the Grain Hill model. The CTS approach, at least as it is defined here, does not lend itself to variations in grain size or geometry. Instead, we introduce an additional type of particle that represents the behavior of blocks rather than treating their difference in size explicitly. In a sense, the approach can be viewed as treating blocks as having greater density, rather than greater size, than other grains. A block particle differs from a normal regolith cell in that it cannot be scattered upward by disturbance. Motion of a block particle can only occur under two circumstances: when it lies directly above an air cell (in which case it falls vertically, trading places with the air cell), and when it lies above and to the side of an air cell (in which case it falls downslope at a 30° angle, with probability per time d). These rules mimic the undermining process discussed by Glade et al. (2017).

As in the Glade et al. (2017) model, block particles can also undergo weathering. Here, weathering is again treated in a probabilistic fashion: blocks form from weathering of bedrock, at probability per time w. Once created, a block can undergo a conversion to normal regolith with probability w when it sits adjacent to an air cell. This treatment of blocks captures, in a simple way, the weathering of blocks as they move down slope. For purposes of this paper, the block component is included simply to test whether a cellular automaton treatment produces results that are qualitatively consistent with observations, and also consistent with the hybrid continuum-discrete model of Glade et al. (2017) and Glade and Anderson (2017).

3 Results

3.1 Fully soil-mantled hillslope

We start by considering the case of fully soil-mantled hillslopes, in which the supply of mobile regolith is effectively unlimited (Figure 2a,b). Under this condition, the Grain Hill model represents a testable mechanistic hypothesis: that a transport-limited, soil-mantled hillslope behaves essentially as a granular medium subject to periodic, quasi-random disturbance events. This concept was also the essence of the acoustic-disturbance experiments by Roering et al. (2001). To test the hypothesis, we run the Grain Hill model with a constant rate of material uplift relative to baselevel until the system reaches ~~steady~~ quasi-steady state, to determine whether its steady form is smoothly convex upward (when the gradient is below the failure threshold) to planar (when the gradient lies at or near the failure threshold). Model runs were performed using a 251-row by 580-column lattice. Disturbance rates were varied from 0.001 yr^{-1} to 0.1 yr^{-1} and intervals between relative-uplift events from 100 to 10,000 yr.

Results show that the Grain Hill model produces parabolic to planar hillslope forms, depending on the ratio of disturbance to uplift rates, which is encapsulated in the dimensionless parameter d' (Figure 8). At high d' (frequent disturbance and/or slow

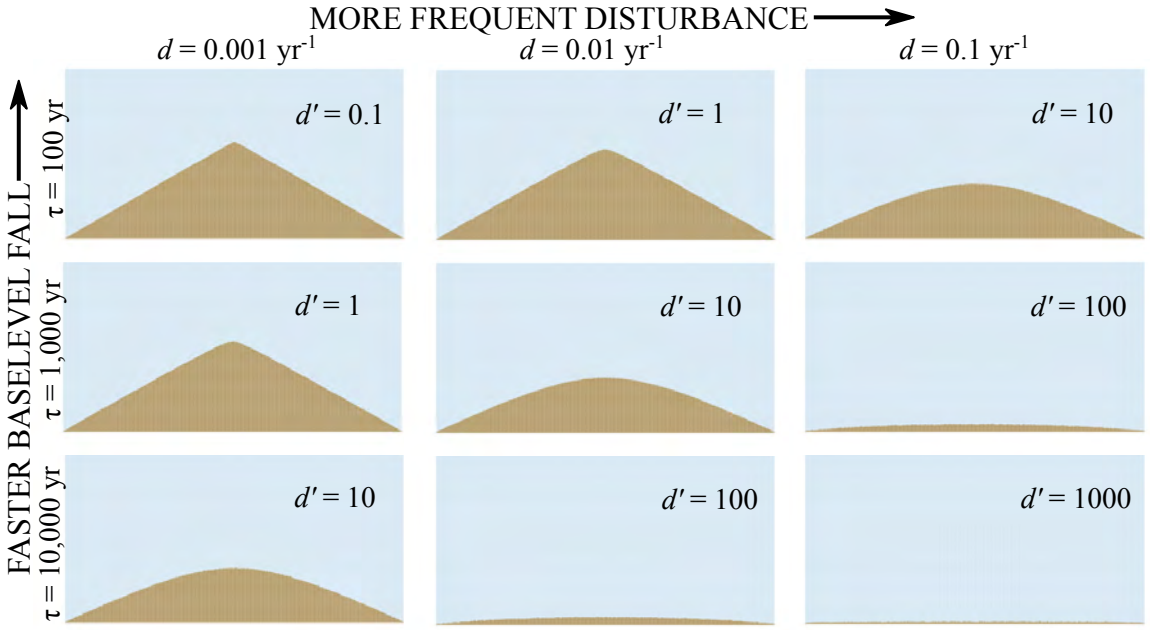

Figure 8. Equilibrium topographic cross-sections using only regolith particles (no rock) and a variety of disturbance frequencies (d) and time interval between baselevel fall events (τ). Fast basal incision and/or infrequent disturbance leads to planar threshold hillslopes; slow basal incision and/or frequent disturbance leads to parabolic hillslopes.

baselevel fall), hillslope relief is low and the form is smoothly convex upward (Figure 8, lower right panels). At somewhat lower d', the lower part of the slope approaches a threshold angle while the upper part remains smoothly convex (Figure 8, middle diagonal panels). At low d', the form becomes predominantly planar and achieves a threshold relief that is insensitive for further increases in d' (Figure 8, upper left panels).

Scaling of mean height as a function of d' is shown in Figure 9. The figure shows results for 125 model runs spanning two orders of magnitude in each parameter (d, τ, and λ) in half-decade intervals. The 125 runs represent a $5 \times 5 \times 5$ grid of experiments, in which each grid point represents a particular combination of the three parameters d, τ, and λ.

For any given hillslope length, there are three regimes of behavior. Low d' (upper left of graph) leads to threshold hillslopes, in which relief depends only on hillslope length. Under moderate d', mean height scales inversely with d', as expected from linear diffusion theory. At high d', we have a finite-size regime in which dimensionless hillslope mean height is comparable to the disturbance scale, δ (cell size in the model); in other words, the hill is only one or a few cells high.

The behavior of the Grain Hill model in its simple, transport-limited configuration can be compared to diffusion theory, which relates volumetric sediment flux per unit contour length, $\mathbf{q}_s$, to topographic gradient:

$$\mathbf{q}_s = -D_s \frac{\partial \eta}{\partial x} \tag{10}$$

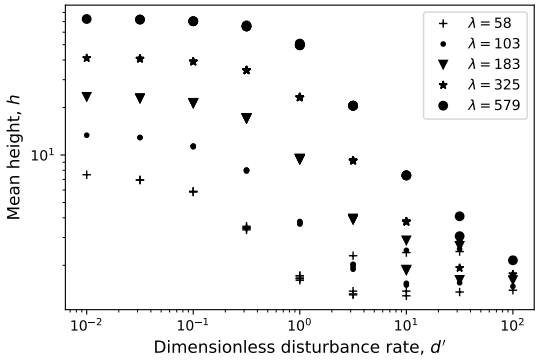

Figure 9. Dimensionless mean hillslope height, h, as a function of dimensionless disturbance rate d' for a range of hillslope lengths. Data points include 125 sensitivity analysis runs in which $d \in [10^{-3}, 10^{-2.5}, 10^{-2}, 10^{-1.5}, 10^{-1}]$, $\tau \in [10^{2}, 10^{2.5}, 10^{3}, 10^{3.5}, 10^{4}]$, and λ as shown in the legend.

where η is land-surface height, x is horizontal distance, and D_s is an effective transport coefficient. The Furbish et al. (2009) probabilistic theory for transport due to particle scattering and settling formulates D_s as

$$D_s = k r_p R_a \overline{N_a \left(1 - \frac{c}{c_m}\right)^2} \cos^2\theta \tag{11}$$

where k is a dimensionless coefficient, r_p is particle radius, R_a is active regolith thickness, N_a is the activation rate, θ is slope angle, c is particle concentration, and c_m is a maximum concentration. The over-bar denotes an average over the active regolith thickness. For the Grain Hill model, R_a scales with the characteristic disturbance depth, δ. Further, because we treat grain aggregates, we may also assume $r_p \sim \delta$. Therefore, we have the prediction that

$$D_s = a \delta^2 N_a \cos^2\theta \tag{12}$$

where a is a dimensionless proportionality constant.

The mean expected activation rate, N_a, is closely related to the Grain Hill model's disturbance frequency parameter, d. To relate the two quantitatively, one needs to make a trivial lattice-geometry correction. A straight-as-possible cut through the hex lattice exposes on average two faces per cell, both of which are susceptible to a disturbance event. Because d is the expected disturbance frequency per cell face, and because independent Poisson events are additive, the resultant disturbance frequency for each cell exposed along a quasi-horizontal surface is $N_a = 2d$.

A more important difference is that whereas N_a is defined as activation rate per unit horizontal area, d represents the rate per unit surface area regardless of orientation. For a given d, N_a will increase with surface roughness (because there is more exposed area of regolith-air contact), and with gradient (because the slope length increases).

An additional effect arises from the model's effective 30° angle of repose. On slopes steeper than this, the expected disturbance rate increases substantially because gravitational dislodgement becomes activated (Figure 5, bottom row). Thus, the

Grain Hill model incorporates an additional nonlinear relationship between flux and gradient inasmuch as N_a depends on gradient.

We can derive an effective diffusivity, D_e, from the modeled topography by applying the expected relationship between mean elevation and diffusivity. Here D_e is defined as that value which, if it were spatially uniform, would yield the same mean steady-state elevation as that produced by the particle model. Framing it this way allows us to interrogate how the effective transport coefficient varies as a function of mean slope gradient. At steady state, mass balance implies that

$$\mathbf{q}_s = Ex \tag{13}$$

where E is the rate of erosion—equal to the rate of material uplift relative to baselevel—and x is horizontal distance from the ridge top. Substituting equation (10) and rearranging,

$$\frac{d\eta}{dx} = -\frac{E}{D_s(x)}x \approx -\frac{E}{D_e}x \tag{14}$$

Integrating and then averaging over x, we can solve for the average elevation, $\overline{\eta}$:

$$\overline{\eta} = \frac{E}{3D_e}L_h^2 \tag{15}$$

where $L_h = L/2$ is the length of the slope from ridge top to base (in other words, half the total length of the domain). We can then rearrange this to find D_e:

$$D_e = \frac{E}{3\overline{\eta}}L_h^2 \tag{16}$$

To examine how D_e scales, we can define a dimensionless form, normalizing by the disturbance frequency, d, and the square of active regolith thickness (equal to particle diameter), δ^2:

$$D_e' = \frac{D_e}{d\delta^2} = \frac{EL_h^2}{3\overline{\eta}d\delta^2} \tag{17}$$

Noting that $E = \delta/\tau$, $L = 2L_h$, and $L/\delta = \lambda$, this is equivalent to

$$D_e' = \frac{\lambda^2}{12\overline{h}d\tau} \tag{18}$$

where $\overline{h}$ is the mean hillslope height in particle diameters.

As expected, D_e' increases with hillslope gradient (Figure 10). The effective diffusivity approaches an asymptote at 30° (~~slope~~ mean gradient ≈0.6), representing an angle of repose. The pattern resembles the family of nonlinear flux-gradient curves introduced by Andrews and Bucknam (1987) and explored further by Howard (1994) and Roering et al. (1999). At low gradients, D_e' approaches a value of about 60. (This method of estimating D_e' is similar to fitting the standard theoretical parabolic curve to the experimental profiles, except that here we use the integral of the profiles.)

The link between D_e and d provides a way to scale the Grain Hill model to field-derived estimates of D_s and R_a. Here we equate the theoretical effective diffusivity, D_e, with the definition of the transport coefficient D_s of Furbish et al. (2009).

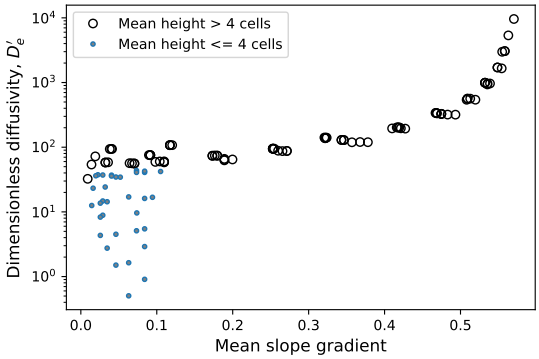

Figure 10. Relationship between dimensionless diffusivity and mean ~~hillslope~~ gradient, from the series of 125 model runs of which a subset are shown in Figure 8.

Noting that at low gradients, $\cos^2\theta$ in equation (12) approaches unity, and using the prior relation $N_a = 2d$, we may write D_s for low slope angle as

$$D_s(\theta \to 0) = 2a\delta^2 d. \tag{19}$$

In the Grain Hill model, the fact that low-angle $D'_e \approx 60$ implies that the dimensional equivalent $D_e(\theta \to 0) \approx 60\delta^2 d$. Equating D_s (the transport coefficient derived by Furbish et al. (2009)) and D_e (the effective transport coefficient derived from the Grain Hill model),

$$D_s(\theta \to 0) \approx 60\delta^2 d. \tag{20}$$

This relation can be used to scale the parameters in the Grain Hill model with field data. For example, if one were to assume an active regolith thickness of 0.4 m and a low-gradient transport coefficient of $D_s = 0.01$ m^2/yr, and set δ to the active regolith thickness, then

$$d = \frac{D_s}{60\delta^2} \approx 0.001 y^{-1}. \tag{21}$$

Here, d represents the frequency with which a given exposed patch of regolith of width and depth δ is disturbed upward. With the above values, the simulated hills in Figure 8 would be 232 m long (valley-to-valley) with height ranging from 1.6 to 57.6 m and baselevel lowering rate from 0.04–4 mm/yr.

3.2 Hillslope with regolith production from rock

Having established that the Grain Hill model reproduces classic soil-mantled hillslope forms and has parameters that can be related to the parameters in commonly used continuum hillslope transport theories, we turn now to the case in which regolith is generated from bedrock with a production rate that may (or may not) limit the rate of erosion. We explore the role of regolith

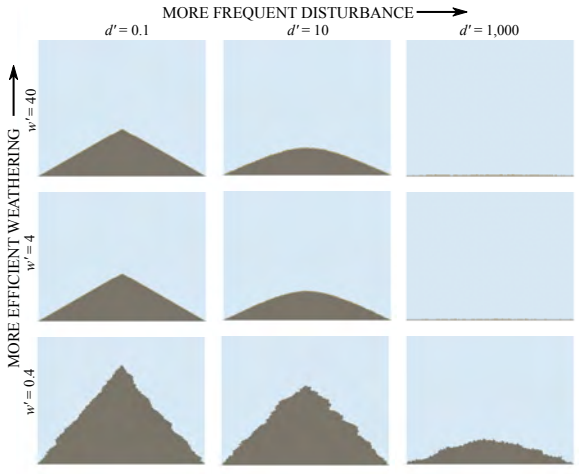

Figure 11. Final equilibrium profiles from Grain Hill runs with rock and weathering. Domain size is 222 rows by 257 columns, and uplift interval ranges from 100 to 10,000 years.

production with a series of model runs in which w' varies from 0.4 to 40. The upper end of this range represents a condition in which the potential maximum rate of regolith production greatly exceeds the rate of baselevel lowering. The lower end, 0.4, is less than the rate of baselevel fall, and would seem to be insufficient to allow for equilibrium to occur, and yet nonetheless it does. Examples of equilibrium hillslope forms found in this parameter space are shown in Figure 11.

Relationships among mean gradient, fractional regolith cover, dimensionless disturbance rate d', and dimensionless weathering rate w' are illustrated in Figure 12. For $w' > 1$, the gradient-d' relation (Figure 12a) has the same shape as in the purely regolith models: a threshold regime at lower d' transitioning to an inverse gradient-d' relation at higher d'. This indicates that when the maximum weathering rate (for a flat surface) is substantially greater than the rate of baselevel fall, we recapture transport-limited conditions. With $w' < 1$, however, the hillslope achieves an equilibrium gradient that is greater than that for the transport-limited case, and at lower d', is greater than the threshold angle (Figures 12a,b).

We can also examine the fractional regolith cover, which is defined here as the number of rock-air cell pairs divided by the total number of cell pairs at which air meets either regolith or rock (Figures 12c,d). The fractional regolith cover shows relatively little sensitivity to d' (Figure 12c). The cover hovers around unity for high w' and d', but systematically declines with w' when w' is below about 10. (Note that the data points representing $d' = 1000$ and $w' > 1$ have hillslope heights of only a few particles, and are therefore sensitive to finite-size effects).

The models with $w' < 1$ present a seeming paradox: how is it possible to achieve an equilibrium form when the maximum weathering rate appears to be lower than the rate of uplift relative to baselevel? The solution to the paradox lies in surface area. The surface area of rock that is exposed to weathering is not fixed, but rather depends on the overall slope length, the terrain roughness, and the fractional regolith cover. To appreciate the first effect, consider a planar slope at angle θ with no regolith cover. If $w\delta$ represents the maximum slope-normal bedrock weathering rate, then the vertical rate is simply $w\delta/\cos\theta$. All

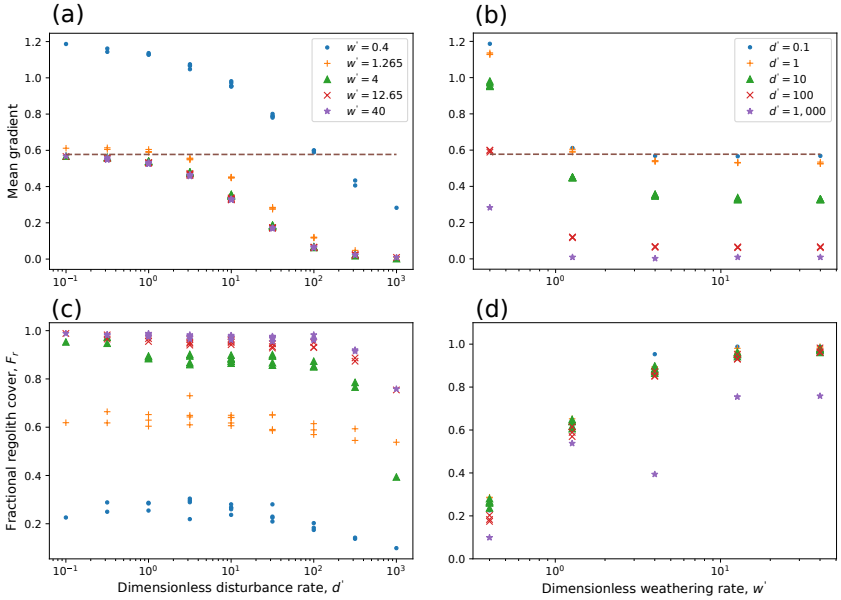

Figure 12. Mean equilibrium gradient and regolith thickness for models with rock and weathering, as a function of d' and w'. Data represent 125 runs with $d \in [10^{-3}, 10^{-2.5}, 10^{-2}, 10^{-1.5}, 10^{-1}]$ y^{-1}, $w' \in [10^{0}, 10^{0.5}, 10^{1}, 10^{1.5}, 10^{2}]$, and $\tau \in [10^{2}, 10^{2.5}, 10^{3}, 10^{3.5}, 10^{4}]$ y.

else equal, increasing gradient will increase vertical weathering rate, thereby providing a feedback between gradient and rock lowering rate. A second feedback relates to topographic roughness: all else equal, a rougher surface will experience a greater weathering rate because it provides more surface area. The third feedback, which is embedded in the depth-dependent regolith production hypothesis (Ahnert, 1967) lies in regolith cover: the greater the exposure of rock (or the thinner the cover), the faster the average rate of rock-to-regolith conversion. In the Grain Hill model, this third feedback is represented by fractional bedrock exposure (since weathering only occurs when rock cells are juxtaposed with air cells).

To test whether these are indeed the feedbacks responsible for equilibrium topography in the Grain Hill model, we can compare the rate of material influx (uplift relative to baselevel) with the expected rate of rock-to-regolith conversion. In the Grain Hill model, the expected rate of regolith production, P, in cross-sectional area per time, is the product of weathering rate per cell face, w, the cross-sectional area of a cell, A, and the number of rock-air cell faces, n_{ra},

$$P = wAn_{ra}, \tag{22}$$

The rate of material addition due to uplift relative to baselevel, U, again in cross-sectional area per time, is the area of a cell, A, times the horizontal width of the domain in cells, n_H, divided by the interval between uplift events, τ:

$$U = n_H A/\tau. \tag{23}$$

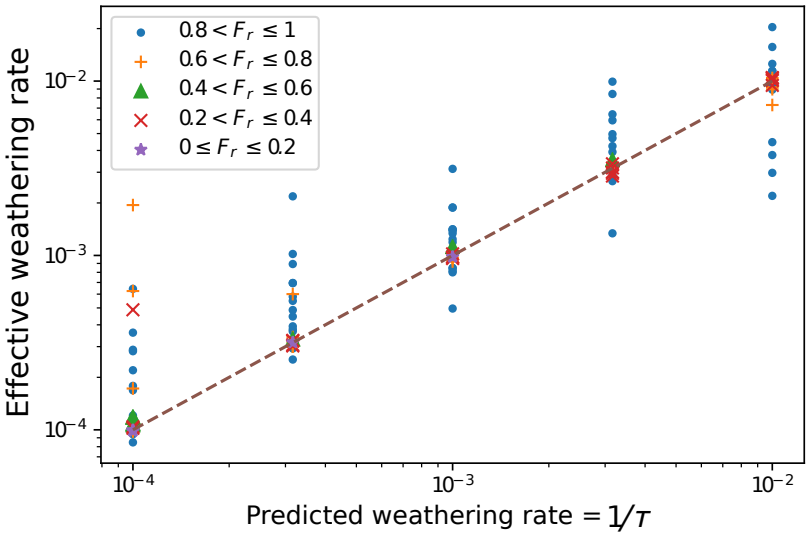

Figure 13. Comparison between rate of material input, $1/\tau$ (cells/year), with effective rate of weathering, wn_{ra}/n_H, from 125 model runs (see text).

Equality between rock uplift and weathering can be expressed as:

$$\frac{1}{\tau} = w\frac{n_{ra}}{n_H}. \tag{24}$$

The ratio on the right side represents the surface-area effect, in the form of surface area exposed to weathering per unit horizontal area. The balance is illustrated in Figure 13, which compares the left-hand and right-hand terms for each of the 125 model runs with weathering. Each data point represents a single snapshot in time, and so scatter is to be expected. To help diagnose the scatter around the 1:1 line, the data are divided into quintiles by fractional regolith cover, F_r (note that some of the points in the lower quintiles are obscured by being over-plotted along the 1:1 line). Many of the points that fall off the 1:1 line, especially at the high end (higher $1/\tau$), come from runs with $F_r > 80\%$; with very few exposed rock-air pairs, a small fluctuation in the n_{ra} can produce a relatively large change in predicted weathering rate. At the low end, many of the points above the 1:1 line come from runs with a maximum height of only a few cells, which are subject to finite-size effects.

The main message of Figure 13 is that the Grain Hill model demonstrates an equilibrium adjustment between rock uplift and rock weathering. The weathering rate does not have a fixed upper "speed limit," but rather is set by the exposed surface area, which in turn is a function of gradient, roughness, and regolith cover. Solutions with a discontinuous regolith cover are indicative of this adjustment. Slopes can grow arbitrarily steep, with weathering and erosion increasingly attacking from the sides as the gradient rises.

3.3 Comparison between weathering rule and inverse-exponential model

The most popular function to describe regolith production from bedrock is the decaying exponential formula proposed by Ahnert (1967), which has proved consistent with estimates of production rate obtained using cosmogenic radionuclides (Heimsath et al., 1997; Small et al., 1999). The production rate is given by:

$$P = P_0 \exp\left(-R/R_*\right), \tag{25}$$

where P_0 is the maximum (bare bedrock) production rate, R is regolith thickness, and R_* is a depth-decay scale on the order of decimeters. On a flat surface, assuming no erosion or deposition, the expected rate of change of R over time is:

$$\frac{dR}{dt} = \frac{\rho_r}{\rho_s}(1-\omega) P_0 \exp\left(-R/R_*\right), \tag{26}$$

where ρ_r and ρ_s are the bulk densities of parent material and regolith, respectively, and ω is the fraction of parent material removed in solution upon weathering. Starting from a bare surface, and assuming isovolumetric weathering (in which case $\rho_s = (1-\omega)\rho_r$), the expected regolith thickness as a function of time can be found by integrating equation (26):

$$\frac{R}{R_*} = \ln\left[\frac{P_0}{R_*}t + 1\right] \tag{27}$$

We can compare this with the behavior of the cellular weathering rule by running the case of a flat, initially bare-rock surface from which weathered material may neither enter nor leave (Figure 14, case $d/w = 0$). When the disturbance rate is zero, the cellular weathering model asymptotically approaches a steady regolith thickness of exactly one cell (thickness = δ). This is so because the model allows weathering to occur only when rock cells are exposed to air cells, and there is no disturbance process that would juxtapose rock and air once the initial weathered layer has formed. When disturbance rate is nonzero, however, regolith continues to form even after the mean thickness r exceeds unity (representing one characteristic disturbance depth). Continuation of regolith production occurs because the disturbance process intermittently exposes rock, at which point it becomes subject to weathering. The greater the disturbance rate, the more frequent the exposure and hence the more rapid weathering (Figure 14). For any ratio d/w, the model's weathering behavior clearly differs from the logarithmic growth in thickness predicted by exponential theory. This represents both a strength and a weakness in the Grain Hill model. On the one hand, the model under its present configuration cannot account for rock-to-regolith conversion resulting from processes that penetrate more than one characteristic disturbance depth δ into the subsurface. For example, the model neglects the possibility that some plant roots may penetrate deeply and contribute to disaggregation, or that an unusually deep freezing front in a cold winter might cause rock fracture and displacement of the resulting fragments (e.g., Anderson et al., 2012). On the other hand, the model honors the likelihood that soil disturbance and regolith production are closely linked processes, rather than being independent: all else equal a greater disturbance rate will tend to produce faster rates of both regolith production and downslope soil movement.

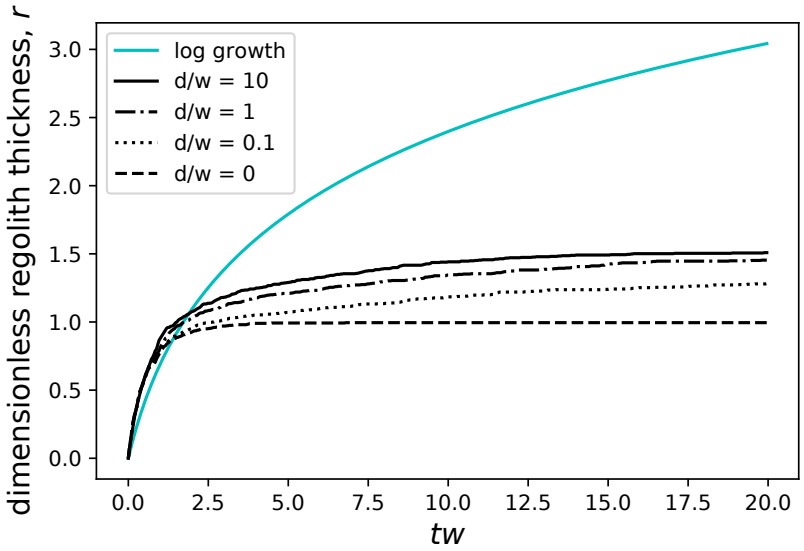

Figure 14. Regolith thickness versus time, as predicted by inverse-exponential theory (log growth; solid cyan curve) and the Grain Hill model with a range of ratios of disturbance rate (d) to weathering rate (w). Time (horizontal axis) is nondimensionalized by multiplying by w.

3.4 Rock collapse and vertical cliffs

Some rock slopes display a cliff-and-rampart morphology in which a vertical or near-vertical rock face stands above an inclined, often sediment-mantled buttress (Figures 1 and 15). Although common in sedimentary rocks where a resistant unit forms the cliff and a weaker unit the buttress, the same morphology is sometimes found in apparently homogeneous lithology (Figure 15b). The cliff portion of such slopes suggests a process of undermining and collapse, with the cliff-forming material being cohesive enough to maintain a vertical face but too weak to support overhangs.

To explore the origins of ramp-and-cliff morphology, we consider a version of the Grain Hill model that adds an extra rule to represent collapse: any rock particle that directly overlies air has the possibility to transition to a falling regolith particle, with the same rate as gravitational transition from resting to falling—in other words, as soon as a rock particle has been undermined, it behaves like cohesionless material.

Under dynamic equilibrium, this rule produces a morphology with slopes that are roughly planar, with alternating vertical and sloping sections and patchy regolith cover (Figure 16). With $w' \leq 1$, gradient and regolith cover depend strongly on w' and show little or no sensitivity to d'. When $w' \ll 1$, the hillslope forms resemble pinnacles. These examples demonstrate two combined feedbacks between weathering and baselevel fall: the surface area susceptible to weathering, and the frequency and magnitude of material collapse through undermining.

The case of transient evolution under a stable baselevel leads to the formation of a regolith-mantled, angle-of-repose ramp (Figure 17). The slope break remains relatively sharp as it retreats headward. The ramp forms as a transport slope. The angle of

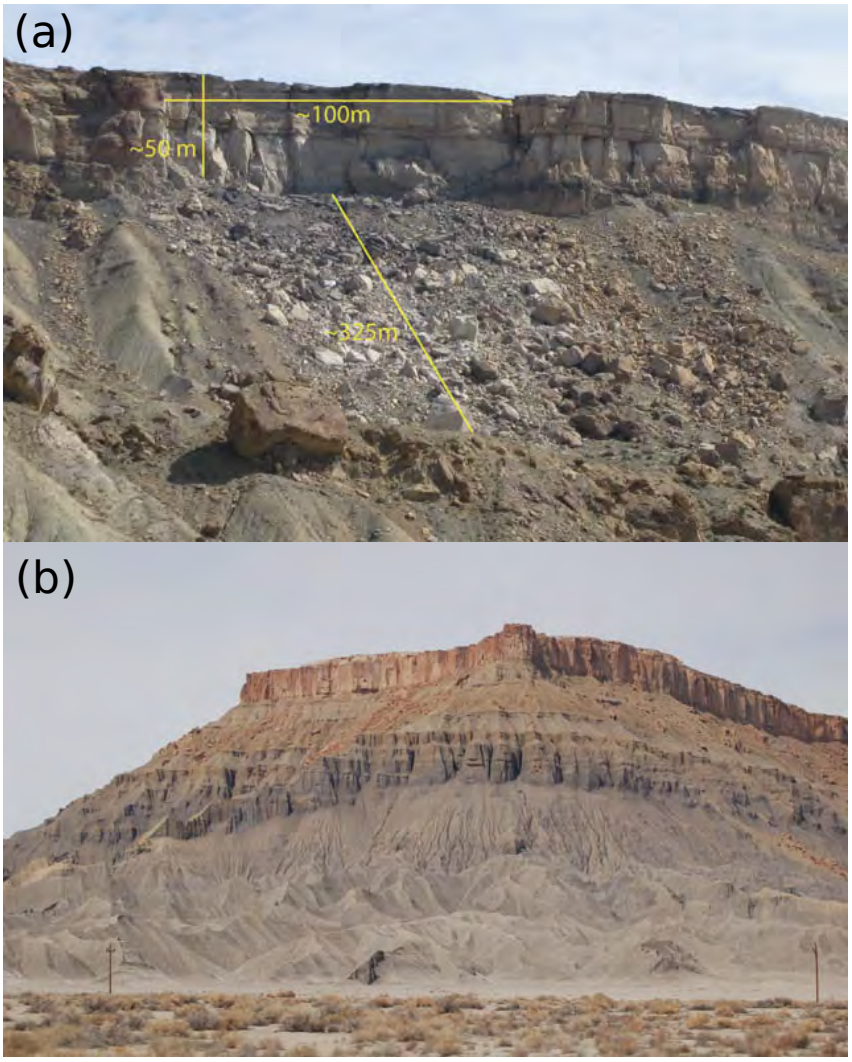

Figure 15. Two examples of cliff-and-rampart morphology. (a) Near Palisade, Colorado, USA, after recent rock-fall event (photo courtesy D.N. Bradley and D. Ward). (b) Colorado Plateau, Utah, USA. Note that contact between lower rampart and sub-vertical slopes, both of which have formed in a gray shale unit, occurs without any apparent break in lithology.

repose is an attractor state: if the angle were steeper, weathered material would be rapidly removed as a result of gravitational instability; if it were substantially lower, material would accumulate, because transport would be limited to the (much lower) rate of disturbance-driven creep motions. Hence, the Grain Hill model predicts that formation of a sediment-mantled ramp beneath a steeper, actively weathering rock slope is an expected outcome for a steep rock slope under stable baselevel.

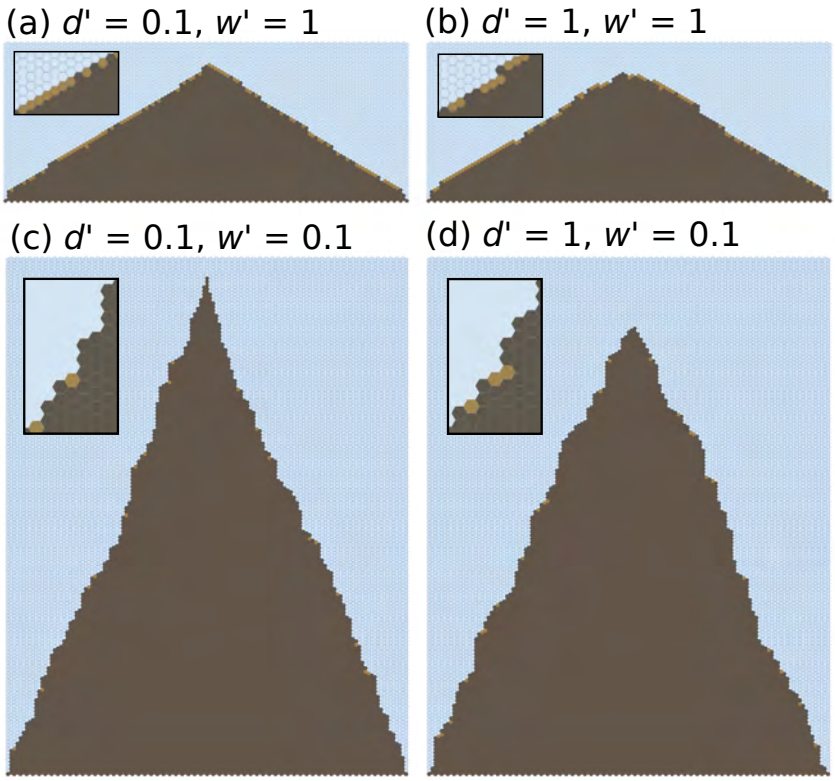

Figure 16. Quasi-steady model hillslope profiles created using a collapse rule, under four different combinations of d' and w'. Insets show magnified views of a portion of each hillslope.

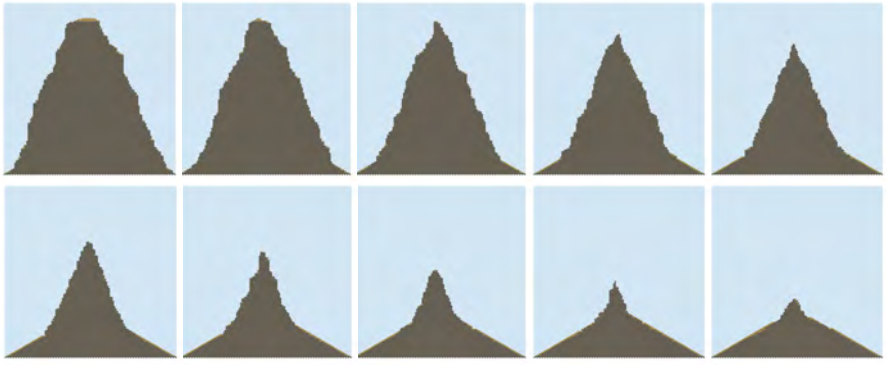

Figure 17. Time series showing transient erosion of a steep rock slope under a stable baselevel, highlighting formation of ramp-and-cliff morphology. Simulation shows 20,000 years of slope evolution under $d = w = 10^{-3}$ y^{-1}. Nominal width, assuming $\delta = 0.1$ m, is 12 m.

3.5 Blocks

Weathering and erosion in landscapes underlain by relatively massive, fracture- or joint-bounded rock can sometimes produce large "blocks" of rock, defined here as clasts that are too large to be displaced upward by normal hillslope processes. The release of blocks from dipping sedimentary or volcanic strata can alter both the shape and relief of hillslopes (Glade et al., 2017). When blocks are delivered to streams, they can influence the channel's roughness, gradient, erosion rate, and longitudinal profile shape (Shobe et al., 2016).

As discussed in Section 2.6, the Grain Hill model can be modified to honor blocks by defining an additional cell type that represents blocks. The weathering process is modified such that a rock cell now weathers into a block, and the block in turn may weather to form regolith. When a block is undermined directly from below, it will fall just as a normal regolith particle would. When a block particle lies adjacent to and above an air cell, a disturbance event may occur that causes the block to shift downward on the slope. By these means, blocks in the model may move downward or downward-and-laterally, but never upward. An implicit assumption in this treatment is that blocks do not roll long distances (further than their own diameter) upon release.

We examine model runs in which a resistant rock layer is embedded in a weak sedimentary material that is soft enough to be treated as regolith (Figure 18). The modeled hillslopes are qualitatively consistent both with field observations and with the mixed continuum-discrete model of Glade et al. (2017) and Glade and Anderson (2017) in that block-mantled slopes are generally concave-upward, reflecting a downslope decrease in the flux of blocks as weathering progressively transmutes them into regolith.

4 Comparison to field sites

We perform a basic validation of the Grain Hill model by comparing its output to real field sites, testing whether the model is capable of reproducing realistic hillslope forms at the correct spatial scale under known boundary conditions. Field sites were chosen such that model boundary conditions could be derived from independent field estimates of rate parameters such as D_s and the rate of baselevel fall. To perform this test, we consider two examples: a convex-upward, soil-mantled hillslope in Gabilan Mesa, California, USA (Figure 2a,b), and a steep, quasi-planar, discontinuously mantled hillslope in the Yucaipa Ridge, California, USA (Figure 2c,d). For each of these two case studies, the hillslopes appear to be approximately at steady state, and independent estimates exist for the rate of baselevel fall, U (Binnie et al., 2007; Perron et al., 2009, 2012). We estimated the effective transport coefficient, D_s, for the profiles shown in Figure 2a,c by measuring the second derivative of the one-dimensional hillslope elevation profiles, $\frac{\partial^2 \eta}{\partial x^2}$, and solving for D_s using

$$D_s = -\frac{U}{\frac{\partial^2 \eta}{\partial x^2}}. \tag{28}$$

For the Gabilan Mesa profile, we estimated the profile-averaged effective transport coefficient as 0.0345 $\mathrm{m^2 y^{-1}}$. The effective rate of baselevel lowering has been estimated at $U \approx 1.47 \times 10^{-4}$ m $\mathrm{y^{-1}}$ (Perron et al., 2012). To construct a Grain Hill model

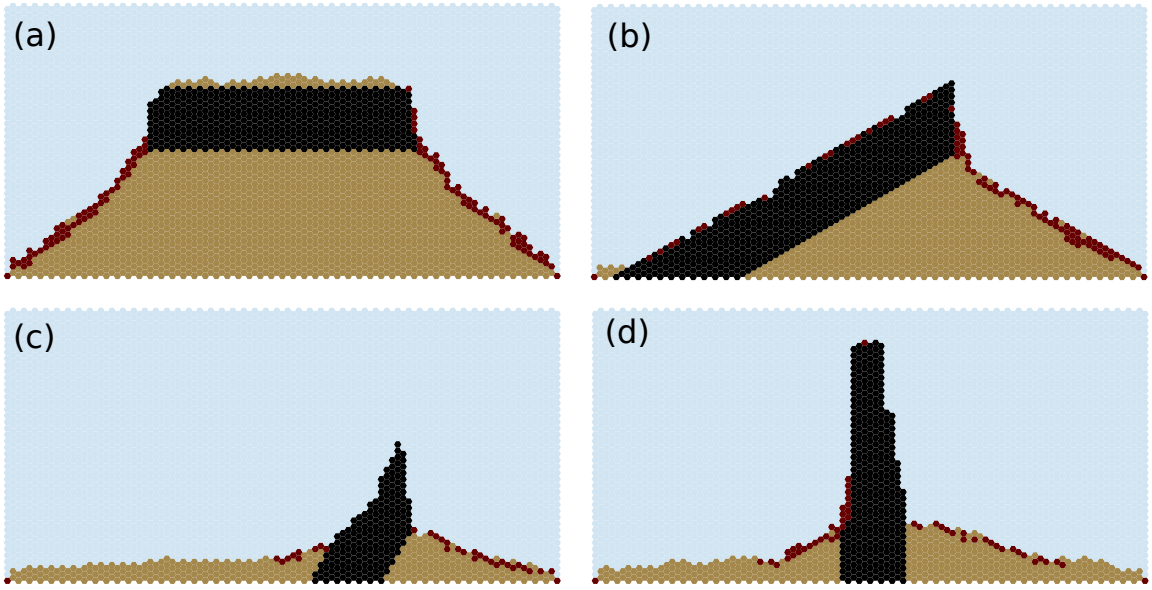

Figure 18. Examples of models that include blocks. Rock (black) weathers to blocks (dark red), which can only move downward or downward-plus-laterally. Blocks in turn weather to regolith (light brown).

for the Gabilan profile, we begin by assuming a characteristic disturbance depth of $\delta = 1$ m. This value was chosen to be consistent with measured soil depths that typically range between 0.2 and 1.2 m (Johnstone et al., 2017). We treat the system as transport-limited, consisting of mobile material, so that weathering is not explicitly modeled. The disturbance parameter, d, is then calculated from the independently estimated value of D_s using equation (20). The interval between uplift events is $\tau = \delta/U \approx 6800$ y. The resulting modeled equilibrium profile provides a reasonably good match to the observed Gabilan profile, with a convex-upward shape and a hilltop height of about 45 m above the slope base (Figure 19a).

For Yucaipa Ridge, we estimated the transport coefficient at $D_s \sim 0.028$ m^{2}y^{-1} on the basis of hilltop curvature and an estimated effective rate of baselevel lowering of $\approx$0.0027 my^{-1} (Binnie et al., 2007). Using equation (20), this equates to a disturbance-rate parameter $d = 0.00468$ y^{-1} and an uplift interval of 370 y in the Grain Hill model. Bedrock outcrops are common on the Yucaipa Ridge hillslopes, implying a thin, discontinuous regolith cover. We therefore treat the system as consisting of bedrock that must be weathered before it can become mobile. Because we do not have independent information on the effective maximum rock weathering rate, the Yucaipa case is a somewhat weaker test: we can only ask whether there exists a geologically reasonable value of w such that the model reproduces the observed relief and shape of the slope profile. Through trial and error, we find that with a weathering rate parameter $w = 0.002$ y^{-1} (which corresponds to a maximum regolith production rate of 2 mm y^{-1}), the model does a credible job of capturing the shape and size of the Yucaipa profile (compare Figure 2c with Figure 19b). Although this particular value was obtained through a simple calibration process, it is at least both geologically reasonable and, as one might expect, somewhat lower than the rate of baselevel lowering.

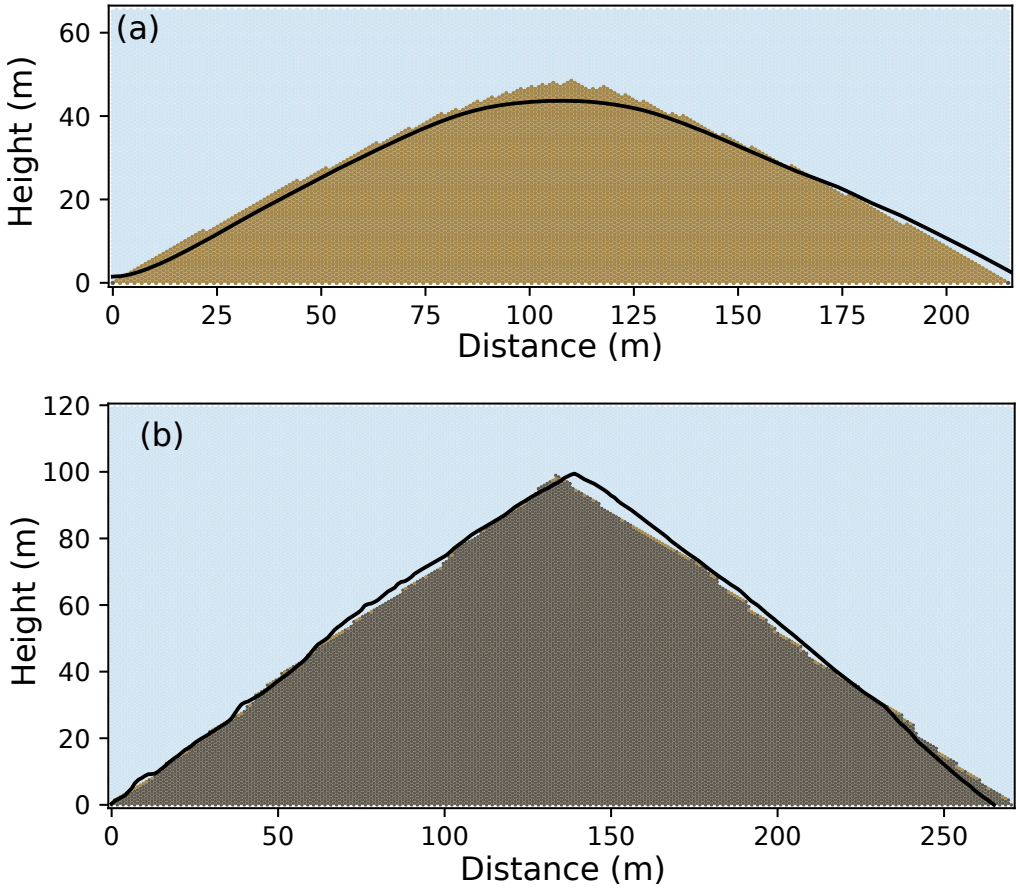

Figure 19. ~~State~~ Steady state models using parameters estimated from observed hillslope profiles. (a) Parameters based on Gabilan Mesa, with the profile shown in Figure 2a,b for comparison. (b) Parameters based on Yucaipa Ridge, with the profile shown in Figure 2c,d for comparison.

To test the sensitivity of the Yucaipa example to the assumed characteristic disturbance depth, we ran a second experiment in which δ was reduced to 0.75 m, and the weathering, disturbance rate, and uplift parameters were re-scaled to accordingly. The relief and mean gradient of the two cases are nearly identical, with planar slopes and a relief in both cases of ~ 100 m.

These two examples demonstrate that the Grain Hill model parameters are not arbitrary, but instead can be linked through straightforward reasoning to field estimates of transport efficiency and baselevel lowering. When one does so, the model successfully reproduces both the shape and scale of observed slopes.

5 Discussion

With just three parameters—disturbance frequency (d), characteristic disturbance depth (δ), and baselevel fall frequency (u)—the Grain Hill algorithm can reproduce the convex-upward to quasi-planar forms associated with soil-mantled hillslopes (Figure 8). With the addition of a parameter that represents rock-to-regolith conversion rate, the algorithm accommodates partly mantled, rocky hillslopes (Figures 11, 16, 17). By adding a rule for detachment of blocks from resistant rock, the model reproduces hillslope forms associated with hogbacks and ledge-forming escarpments (Figure 18).

A common criticism of cellular automaton models is that they involve arbitrary rules and/or parameters that can neither be measured nor verified in the real world. That is not the case for the Grain Hill model, for which the parameters are tied to measurable physical quantities. For example, the disturbance frequency d is directly related to the frequency parameter N_a in statistical theory of soil transport developed by Furbish et al. (2009), and through that theory to the diffusion-like transport coefficient D_s that is commonly estimated in field studies. This connection between model parameters and field measurements is illustrated by the model's ability to reproduce the correct shape and scale of observed hillslope forms when estimates of D_s and U are available (Figures 2, 19). In the transport-limited case, there are no tunable parameters: given independent estimates of D_s and U, the correct morphology is recovered (Figure 2a, 19a). In the case where rock weathering appears to play a role, and an independent estimate of P_0 is not available, the model requires an estimation of maximum weathering rate w. Nonetheless, a plausible value of w (0.002 m y^{-1}), somewhat smaller than the rate of baselevel fall (0.0027 m y^{-1}), reproduces the observed shape and relief in the Yucaipa Ridge case study.

The transport dynamics predicted by the Grain Hill model are consistent with continuum soil-transport theory, which treats soil as a fluid with a downslope flow rate that depends on slope gradient. Like the popular Andrews-Bucknam nonlinear transport law (e.g., Andrews and Bucknam, 1987; Howard, 1994; Roering et al., 1999), the transport-limited form of the Grain Hill model predicts diffusion-like behavior in which the effective diffusivity increases with slope gradient, with an asymptote at a threshold angle (Figure 10). In one sense, the Grain Hill model is actually closer to the process level than fluid-like continuum models, because net downslope mass flux arises from a sequence of stochastic disturbance events rather than being dictated by a macroscopic transport law.

One limitation of the Grain Hill model is that its threshold-like behavior arises from the lattice geometry: regolith cells perched at a 30° angle above and to one side of an air cell are treated as unconditionally unstable. Whereas the timing of motion is treated as a stochastic process, the occurrence of motion is inevitable (unless some other event occurs first). This treatment neglects the possibility of frictional locking among noncohesive grains at angles somewhat above 30°, as well as the possibility of cohesion. This limitation could be overcome by introducing a probabilistic treatment of grain stability: a grain aggregate will be stable with a given probability p, and unstable with probability $1 - p$. Such a treatment would introduce an additional parameter, but this parameter could in principle be estimated from physical experiments. The addition of a "sticking rule" like this might also make it possible for models with alternative lattice geometries to manifest the same dynamics, thereby de-coupling the basic model framework from the geometry of the lattice on which it is implemented.

The inclusion of rock-to-regolith conversion enables the Grain Hill model to predict a continuum of slope forms from fully soil mantled to intermittently covered to bare. However, there are several limitations in the treatment of regolith production that could be improved on. The weathering rule assumes that regolith production can only occur when rock is exposed to air, which obviously neglects the role of shallow subsurface processes such as root or frost wedging. The effective weathering depth scale is the same as the disturbance scale, and equal to the cell size. This assumption is probably reasonable if the processes responsible for weathering and disturbance were one and the same, but not if they are distinct processes with different length scales. The Grain Hill model also does not account explicitly for chemical weathering, which in some cases can extend well below the surface. Finally, the model's effective regolith-production behavior does not follow the log-growth curve predicted by inverse-exponential theory for a stable surface (Figure 14). With these caveats in mind, one advantage of the stochastic model of regolith production is that it effectively treats the disturbance and regolith-production processes as being closely linked: all else equal, the production rate is higher when disturbance is more frequent.

The popular inverse-exponential model for regolith production implies the existence of a speed limit to landscape evolution: in the absence of rock landsliding, erosion rate cannot exceed the maximum rate of rock-to-regolith conversion. Moreover, the model implies the existence of a bare landscape once the rate of erosion exceeds the maximum rate of regolith production. Heimsath et al. (2012) found evidence, however, that in fact there are additional stabilizing mechanisms, and that these manifest in landscapes with thin, patchy soils. The Grain Hill model is consistent with these observations in that it predicts the natural emergence of a discontinuous regolith cover, with the fractional cover exerting an influence on the average rate of weathering and erosion. Furthermore, the model behavior highlights the importance of slope length and roughness in modulating the regolith production rate: all else equal, steeper or rougher slopes allow higher production rates, leading to an additional feedback between relief and erosion rate for rocky hillslopes. The possibility of rock collapse upon undermining by weathering provides ~~an additional~~ another feedback mechanism that may allow rates of erosion to exceed the flat-surface maximum regolith production rate (Figure 16).

The Grain Hill model also provides insight into transient evolution of rocky slopes. Experiments on the relaxation of rocky slopes that are steeper than the threshold angle predict the formation of a regolith-mantled pediment at the angle of repose, which extends upslope as the steep upper slope gradually recedes (Figure 17). This scarp-pediment morphology emerges without any variation in material strength, requiring only a period of baselevel stability.

As a computational framework for exploring hillslope forms, the Grain Hill model has the advantage that it provides a mechanistic link between events (disturbance and weathering) and long-term morphologic evolution, without the need to specify a flux law. The model has the further advantage of being fully two dimensional, allowing disturbance and weathering events to initiate from the side as well as vertically. A further key element is that the model can mix timescales: a short timescale associated with grain motion, an intermediate time scale associated with disturbance events, and a much longer timescale for slope evolution. Mixing these disparate timescales in a single computer model is made possible by the fact that most of the time grains are stationary: the algorithm operates on small (stochastic) time steps during those moments when grains are moving, and on much longer steps when no grains are in motion (for further information on the discrete-event algorithm behind the model, see Tucker et al. (2016)).

The Grain Hill framework has several important limitations. It is not practical to simulate motion of individual grains unless the spatial scale is quite limited (e.g., Figure 6) or the grains are unusually large (Figure 18). If one wished to model individual grains (of order say 10^{-3} m) at the scale of a hillslope (of order 10^2 m), a much more efficient solution algorithm would be needed. Furthermore, the nature of a cellular automaton is such that physical interactions are limited to adjacent cells only; long-distance effects such as stress transmission cannot easily be represented. In one sense, the restriction to short-range influence could be seen as an advantage, in that it forces one to think about how it is that mass or energy is actually transmitted in a granular medium. But the restriction means that well-known principles such as solid-state stress cannot easily be represented. On the other hand, the model does capture non-local transport, in which particles set in motion can travel a distance comparable to the slope length (Foufoula-Georgiou et al., 2010; Tucker and Bradley, 2010; Furbish and Roering, 2013). Nonlocal transport emerges in the Grain Hill model when the slope angle is near or above 30°, such that there is a high probability that a disturbed particle will land in an unstable location and continue moving without the need for a second disturbance event.

A further limitation concerns the fixed cell size. Because the model is restricted to a fixed cell size, the Grain Hill framework does not lend itself to treatment of multiple grain sizes (apart from the simple "aggregates and blocks" approach illustrated in Figure 18). Despite these limitations, the Grain Hill model provides a useful framework for exploring hillslope process and form in the context of stochastic events.

6 Conclusions

A continuous-time stochastic cellular automaton model known as the Grain Hill model allows for computational simulation of two-dimensional slope forms that arise from stochastic disturbance and (possibly) weathering events. The model operates on a hexagonal lattice, with cell states representing fluid, rock, and grain aggregates that are either stationary or in a state of motion in one of the six cardinal lattice directions. An optional additional state represents unusually large grains ("blocks") that cannot be displaced upward by disturbance events.

The Grain Hill model is able to reproduce a range of common slope forms, from fully soil mantled to rocky and partially mantled. The bestiary of forms that the model can produce includes convex-upward soil mantled slopes, planar slopes (bare, soil mantled, or in between), and cliffs with basal ramparts. When the model is configured to include a resistant rock layer that decomposes into blocks, the model reproduces observed hogback-like slope forms and qualitatively matches the behavior predicted by a recent continuum-discrete model (Glade et al., 2017; Glade and Anderson, 2017).

In its simplest guise, the model has only three process parameters, which represent disturbance frequency, characteristic disturbance depth, and baselevel lowering rate, respectively. Incorporating physical weathering of rock adds one additional parameter, representing the characteristic rock weathering rate. These parameters are not arbitrary but rather have a direct link with corresponding parameters in continuum theory. Comparison between observed and modeled slope forms demonstrates that the model can reproduce both the shape and scale of real hillslope profiles.

Experiments with the Grain Hill model highlight the importance of regolith cover fraction in governing both the downslope mass transport rate and the rate of physical weathering. Equilibrium rocky hillslope profiles are possible even when the rate

of baselevel lowering exceeds the nominal bare-rock weathering rate, because increases in both slope gradient and roughness can allow for rock weathering rates that are greater than the flat-surface maximum. Finally, experiments in transient relaxation of steep, rocky slopes predict the formation of a regolith-mantled pediment that migrates headward through time while maintaining a sharp slope break.

Author contributions. The idea to develop a 2D cellular rock-slope model arose from conversations among all three authors. The model code was written in Landlab by GT. Both GT and DEJH contributed to the underlying grid data structures and Python code. SWM extracted the hillslope profiles and estimated the parameters for the two field sites. GT performed the computational experiments and wrote the paper, with input and editing from SWM and DEJH.

Acknowledgements. This research was supported by the US National Science Foundation (EAR-1349390 and ACI-1450409 to GT and DEJH, and EAR-1349229 to SWM). DEJH's participation was also supported in part by the National Center for Earth Surface Dynamics (EAR-1246761). Support for high-performance computing and software development was provided by the Community Surface Dynamics Modeling System (CSDMS) (EAR-1226297). High-resolution topographic data was downloaded from Open Topography (http://www.opentopography.org/).

References

Ahnert, F.: The role of the equilibrium concept in the interpretation of landforms of fluvial erosion and deposition, Proc. symp. l'évolution des versants (Liége), 50, 23–51, 1967.

Alonso, J. and Herrmann, H.: Shape of the tail of a two-dimensional sandpile, Physical review letters, 76, 4911, doi: http://dx.doi.org/10.1103/PhysRevLett.76.4911, 1996.

Anderson, R. S., Anderson, S. P., and Tucker, G. E.: Rock damage and regolith transport by frost: An example of climate modulation of the geomorphology of the critical zone, Earth Surface Processes and Landforms, 2012.

Andrews, D. and Bucknam, R. C.: Fitting degradation of shoreline scarps by a nonlinear diffusion model, Journal of Geophysical Research, 92, 12 857–12, 1987.

Binnie, S. A., Phillips, W. M., Summerfield, M. A., and Fifield, L. K.: Tectonic uplift, threshold hillslopes, and denudation rates in a developing mountain range, Geology, 35, 743–746, https://doi.org/10.1130/G23641A.1, http://geology.gsapubs.org/content/35/8/743.abstract, 2007.

Chen, S. and Doolen, G. D.: Lattice Boltzmann method for fluid flows, Annual review of fluid mechanics, 30, 329–364, 1998.

Cottenceau, G. and Désérable, D.: Open environment for 2d lattice-grain CA, in: Cellular Automata, pp. 12–23, Springer, 2010.

Coyote, W. E.: Fast and furry-ous: exploring the links between gravitational forces and situational awareness, Ph.D. thesis, Acme Technical College, 1949.

Culling, W.: Soil creep and the development of hillside slopes, The Journal of Geology, pp. 127–161, 1963.

Culling, W.: Theory of erosion on soil-covered slopes, The Journal of Geology, pp. 230–254, 1965.

Désérable, D.: A versatile two-dimensional cellular automata network for granular flow, SIAM Journal on Applied Mathematics, pp. 1414–1436, 2002.

Désérable, D., Dupont, P., Hellou, M., and Kamali-Bernard, S.: Cellular automata in complex matter, Complex Systems, 20, 67, 2011.

Drake, T. G. and Calantoni, J.: Discrete particle model for sheet flow sediment transport in the nearshore, Journal of Geophysical Research: Oceans, 106, 19 859–19 868, 2001.

Duszyński, F. and Migoń, P.: Boulder aprons indicate long-term gradual and non-catastrophic evolution of cliffed escarpments, Stołowe Mts, Poland, Geomorphology, 250, 63–77, 2015.

Foufoula-Georgiou, E., Ganti, V., and Dietrich, W.: A nonlocal theory of sediment transport on hillslopes, J. Geophys. Res, 115, F00A16, 2010.

Furbish, D. and Haff, P.: From divots to swales: Hillslope sediment transport across divers length scales, Journal of Geophysical Research, 115, F03 001, 2010.

Furbish, D., Hamner, K., Schmeeckle, M., Borosund, M., and Mudd, S.: Rain splash of dry sand revealed by high-speed imaging and sticky paper splash targets, J. Geophys. Res, 112, F01 001, 2007.

Furbish, D., Haff, P., Dietrich, W., and Heimsath, A.: Statistical description of slope-dependent soil transport and the diffusion-like coefficient, J. Geophys. Res, 114, F00A05, 2009.

Furbish, D. J. and Roering, J. J.: Sediment disentrainment and the concept of local versus nonlocal transport on hillslopes, Journal of Geophysical Research: Earth Surface, 118, 937–952, 2013.

Furbish, D. J. and Schmeeckle, M. W.: A probabilistic derivation of the exponential-like distribution of bed load particle velocities, Water Resources Research, 49, 1537–1551, 2013.

Gabet, E.: Sediment transport by dry ravel, Journal of Geophysical Research, 108, 2049, 2003.

Gabet, E. J. and Mendoza, M. K.: Particle transport over rough hillslope surfaces by dry ravel: Experiments and simulations with implications for nonlocal sediment flux, Journal of Geophysical Research: Earth Surface, 117, 2012.

Ghil, M., Zaliapin, I., and Coluzzi, B.: Boolean delay equations: A simple way of looking at complex systems, Physica D: Nonlinear Phenomena, 237, 2967–2986, 2008.

Glade, R. and Anderson, R.: Quasi-steady evolution of hillslopes in layered landscapes: An analytic approach, Journal of Geophysical Research: Earth Surface, 2017.

Glade, R. C., Anderson, R. S., and Tucker, G. E.: Block-controlled hillslope form and persistence of topography in rocky landscapes, Geology, 45, 311–314, 2017.

Gutt, G. and Haff, P.: An automata model of granular materials, in: Proceedings of the fifth distributed memory computing conference, 1990.

Heimsath, A., Dietrich, W., Nishiizumi, K., and Finkel, R.: The soil production function and landscape equilibrium, Nature, 388, 358–361, 1997.

Heimsath, A., DiBiase, R., and Whipple, K.: Soil production limits and the transition to bedrock-dominated landscapes, Nature Geoscience, 5, 210–214, 2012.

Hobley, D. E., Adams, J. M., Nudurupati, S. S., Hutton, E. W., Gasparini, N. M., Istanbulluoglu, E., and Tucker, G. E.: Creative computing with Landlab: an open-source toolkit for building, coupling, and exploring two-dimensional numerical models of Earth-surface dynamics, Earth Surface Dynamics, 5, 21, 2017.

Howard, A. D.: A detachment-limited model of drainage basin evolution, Water Resources Research, 30, 2261–2285, 1994.

Howard, A. D. and Selby, M. J.: Rock Slopes, in: Geomorphology of Desert Environments, pp. 123–172, Springer, 1994.

Johnstone, S. A., Chadwick, K. D., Frias, M., Tagliaro, G., and Hilley, G. E.: Soil Development over Mud-Rich Rocks Produces Landscape-Scale Erosional Instabilities in the Northern Gabilan Mesa, Geological Society of America Bulletin, 129, 1266–79, 2017.

Károlyi, A. and Kertész, J.: Lattice-gas model of avalanches in a granular pile, Physical Review E, 57, 852, 1998.

Károlyi, A. and Kertész, J.: Granular medium lattice gas model: the algorithm, Computer physics communications, 121, 290–293, 1999.

Károlyi, A., Kertész, J., Havlin, S., Makse, H. A., and Stanley, H. E.: Filling a silo with a mixture of grains: friction-induced segregation, EPL (Europhysics Letters), 44, 386, 1998.

Lamb, M. P., Scheingross, J. S., Amidon, W. H., Swanson, E., and Limaye, A.: A model for fire-induced sediment yield by dry ravel in steep landscapes, Journal of Geophysical Research: Earth Surface, 116, 2011.

Lamb, M. P., Levina, M., DiBiase, R. A., and Fuller, B. M.: Sediment storage by vegetation in steep bedrock landscapes: Theory, experiments, and implications for postfire sediment yield, Journal of Geophysical Research: Earth Surface, 118, 1147–1160, 2013.

MacVicar, B., Parrott, L., and Roy, A.: A two-dimensional discrete particle model of gravel bed river systems, Journal of Geophysical Research: Earth Surface, 111, 2006.

Martinez, J. and Masson, S.: Lattice grain models, pp. 556–563, E & FN Spon, 1998.

McEwan, I. and Heald, J.: Discrete particle modeling of entrainment from flat uniformly sized sediment beds, Journal of Hydraulic Engineering, 127, 588–597, 2001.

Narteau, C., Le Mouël, J., Poirier, J., Sepúlveda, E., and Shnirman, M.: On a small-scale roughness of the core–mantle boundary, Earth and Planetary Science Letters, 191, 49–60, 2001.

Narteau, C., Zhang, D., Rozier, O., and Claudin, P.: Setting the length and time scales of a cellular automaton dune model from the analysis of superimposed bed forms, Journal of Geophysical Research: Earth Surface (2003–2012), 114, 2009.

Peng, G. and Herrmann, H. J.: Density waves of granular flow in a pipe using lattice-gas automata, Physical Review E, 49, R1796, 1994.

Perron, J. T., Kirchner, J. W., and Dietrich, W. E.: Formation of evenly spaced ridges and valleys, Nature, 460, 502–505, 2009.

Perron, J. T., Richardson, P. W., Ferrier, K. L., and Lapôtre, M.: The Root of BBranching River Networks, Nature, 492, 100–103, 2012.

Roering, J.: Soil creep and convex-upward velocity profiles: Theoretical and experimental investigation of disturbance-driven sediment transport on hillslopes, Earth Surface Processes and Landforms, 29, 1597–1612, 2004.

Roering, J.: How well can hillslope evolution models "explain" topography? Simulating soil transport and production with high-resolution topographic data, Geological Society of America Bulletin, 120, 1248–1262, 2008.

Roering, J., Kirchner, J., and Dietrich, W.: Evidence for nonlinear, diffusive sediment transport on hillslopes and implications for landscape morphology, WATER RESOURCES RESEARCH, 35, 853–870, 1999.

Roering, J., Kirchner, J., Sklar, L., and Dietrich, W.: Hillslope evolution by nonlinear creep and landsliding: An experimental study, GEOLOGY, 29, 143–146, 2001.

Roering, J. J. and Gerber, M.: Fire and the evolution of steep, soil-mantled landscapes, Geology, 33, 349–352, 2005.

Rozier, O. and Narteau, C.: A real-space cellular automaton laboratory, Earth Surface Processes and Landforms, 39, 98–109, 2014.

Schmeeckle, M. W.: Numerical simulation of turbulence and sediment transport of medium sand, Journal of Geophysical Research: Earth Surface, 119, 1240–1262, 2014.

Shobe, C. M., Tucker, G. E., and Anderson, R. S.: Hillslope-derived blocks retard river incision, Geophysical Research Letters, 43, 5070–5078, 2016.

Small, E., Anderson, R., and Hancock, G.: Estimates of the rate of regolith production using 10Be and 26Al from an alpine hillslope, Geomorphology, 27, 131–150, 1999.

Tucker, G. and Bradley, D.: Trouble with diffusion: Reassessing hillslope erosion laws with a particle-based model, J. Geophys. Res, 115, 2010.

Tucker, G. E., Hobley, D. E., Hutton, E., Gasparini, N. M., Istanbulluoglu, E., Adams, J. M., and Nudurupati, S. S.: CellLab-CTS 2015: continuous-time stochastic cellular automaton modeling using Landlab, Geoscientific Model Development, 9, 823–839, 2016.

Zhang, D., Narteau, C., and Rozier, O.: Morphodynamics of barchan and transverse dunes using a cellular automaton model, Journal of Geophysical Research: Earth Surface (2003–2012), 115, 2010.

Zhang, D., Narteau, C., Rozier, O., and du Pont, S. C.: Morphology and dynamics of star dunes from numerical modelling, Nature Geoscience, 5, 463–467, 2012.